Appendix A

Design for the Main Chamber

This appendix includes the engineering schematics for the main vacuum chamber.

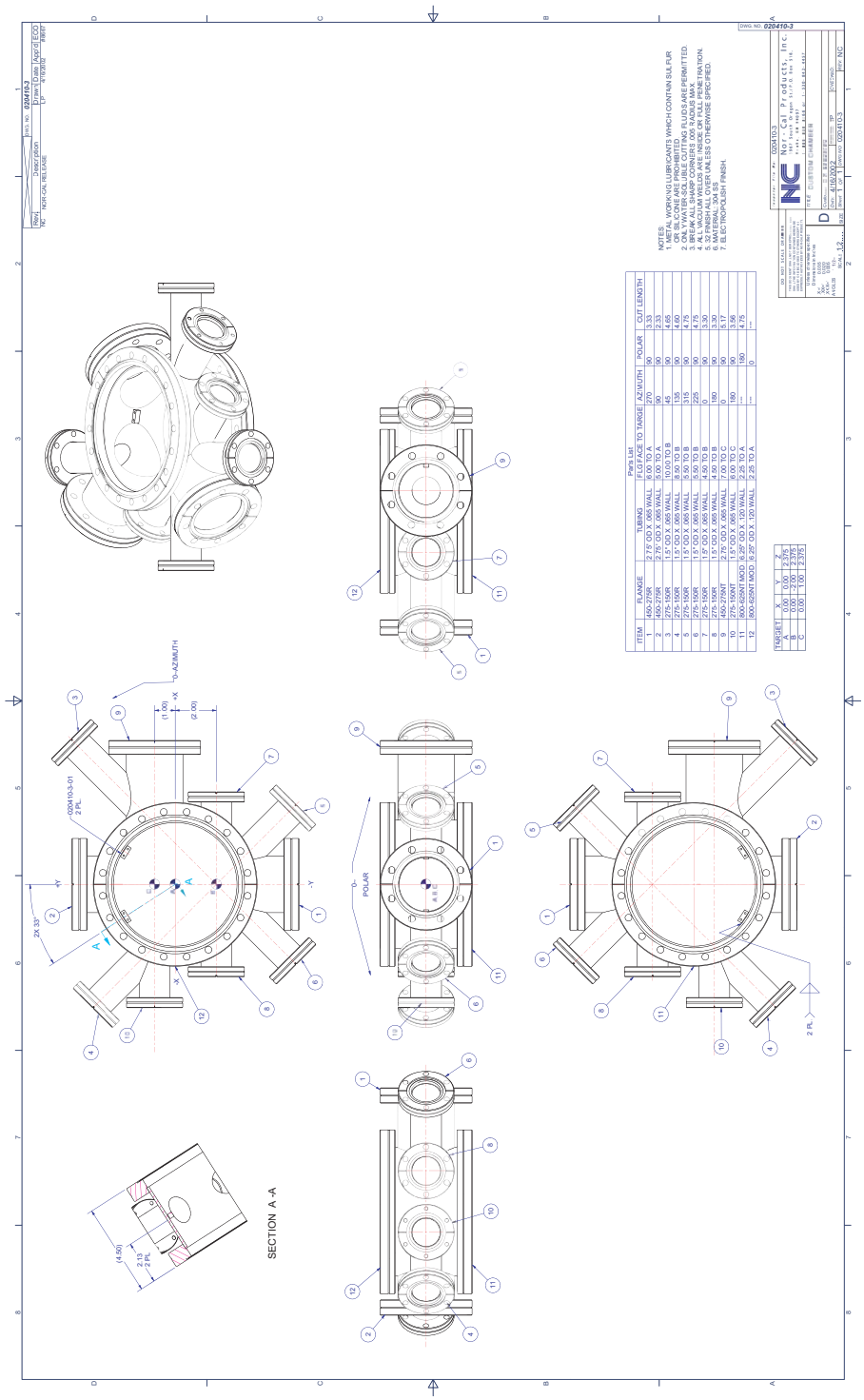

Figure A.1: The main chamber. Drawing generated by Nor-Cal USA.

Appendix B

Designs for the Magnetic Transfer System

This appendix includes the engineering schematics for the magnetic transfer system, including the reentrant bucket, the coil dimensions and layouts, and the mounting bracket.

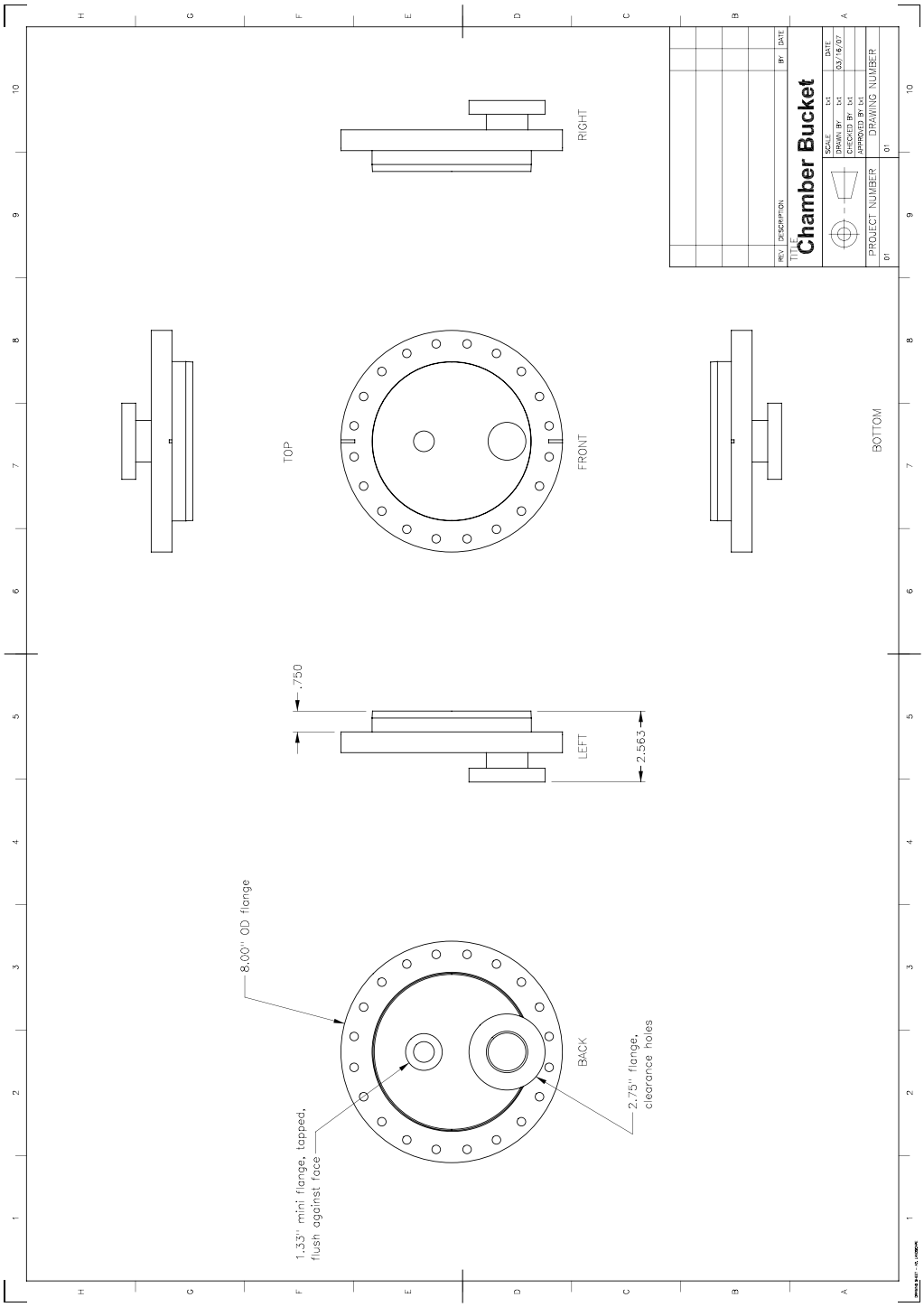

Figure B.1: The reentrant bucket.

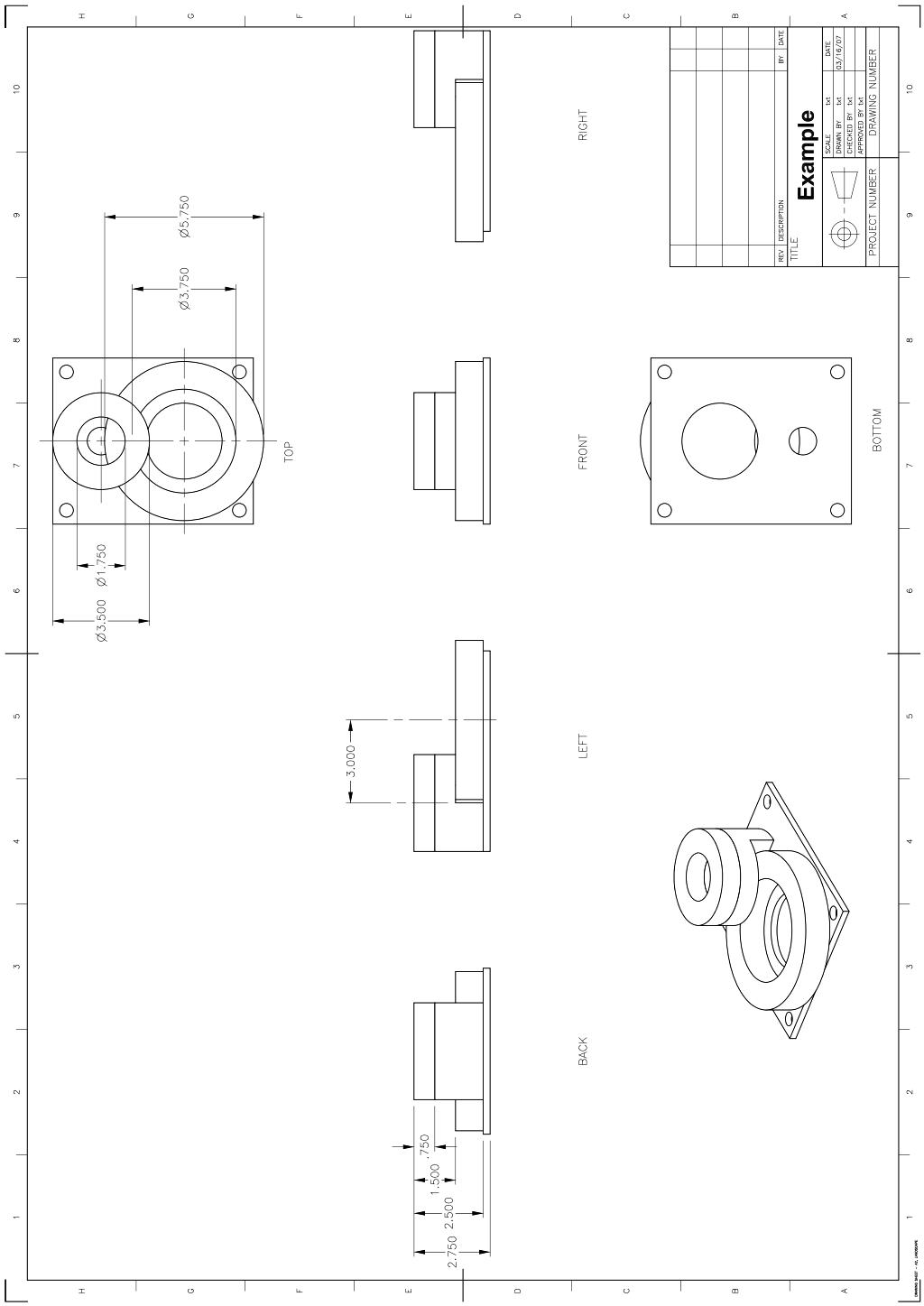

Figure B.2: The magnetic transfer coils.

Appendix C

Designs for the Millitap

This appendix includes the engineering schematics for the millitrap mount pieces.

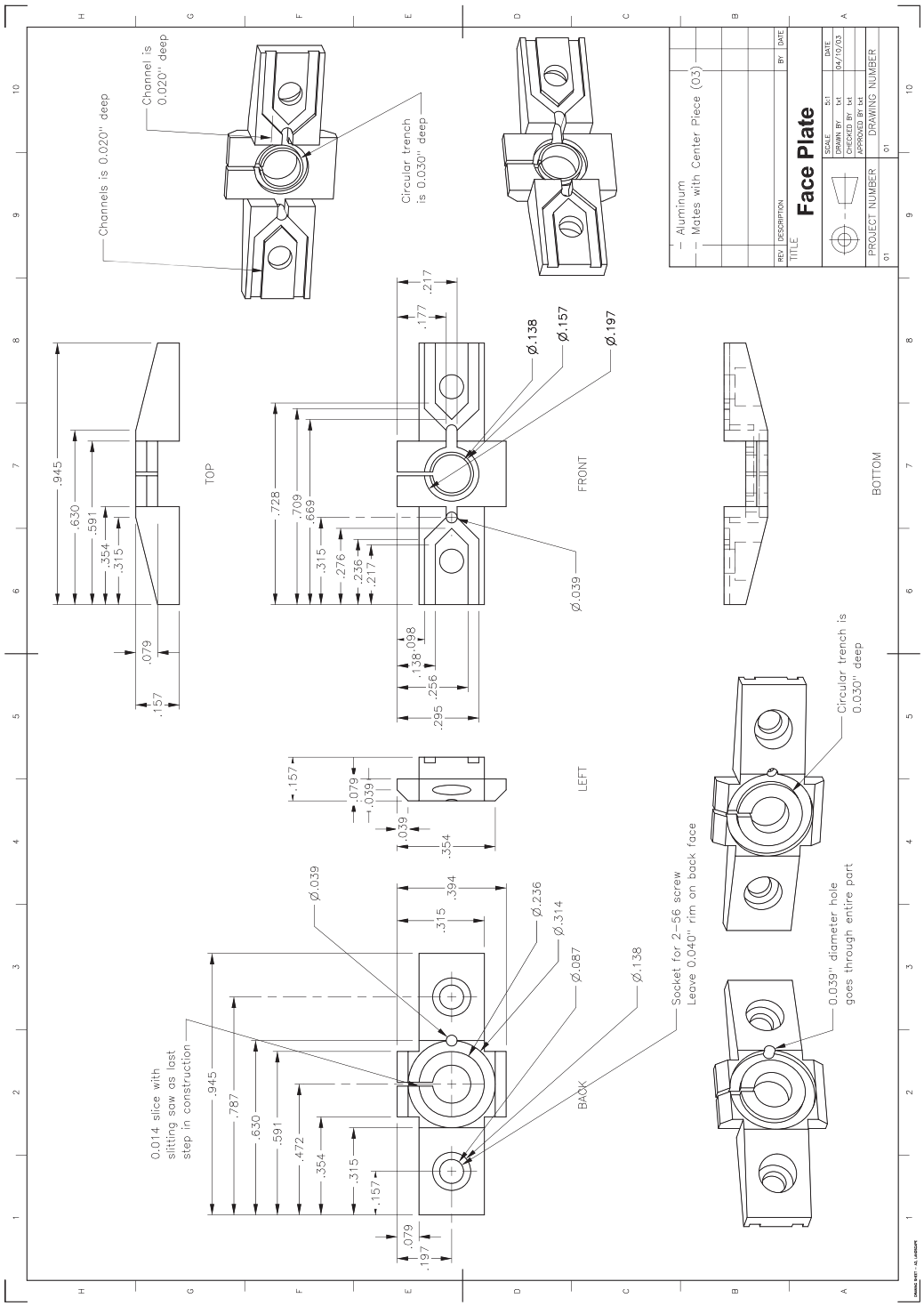

Figure C.1: The mounting plate for the millitrap curvature and anti-bias coils.

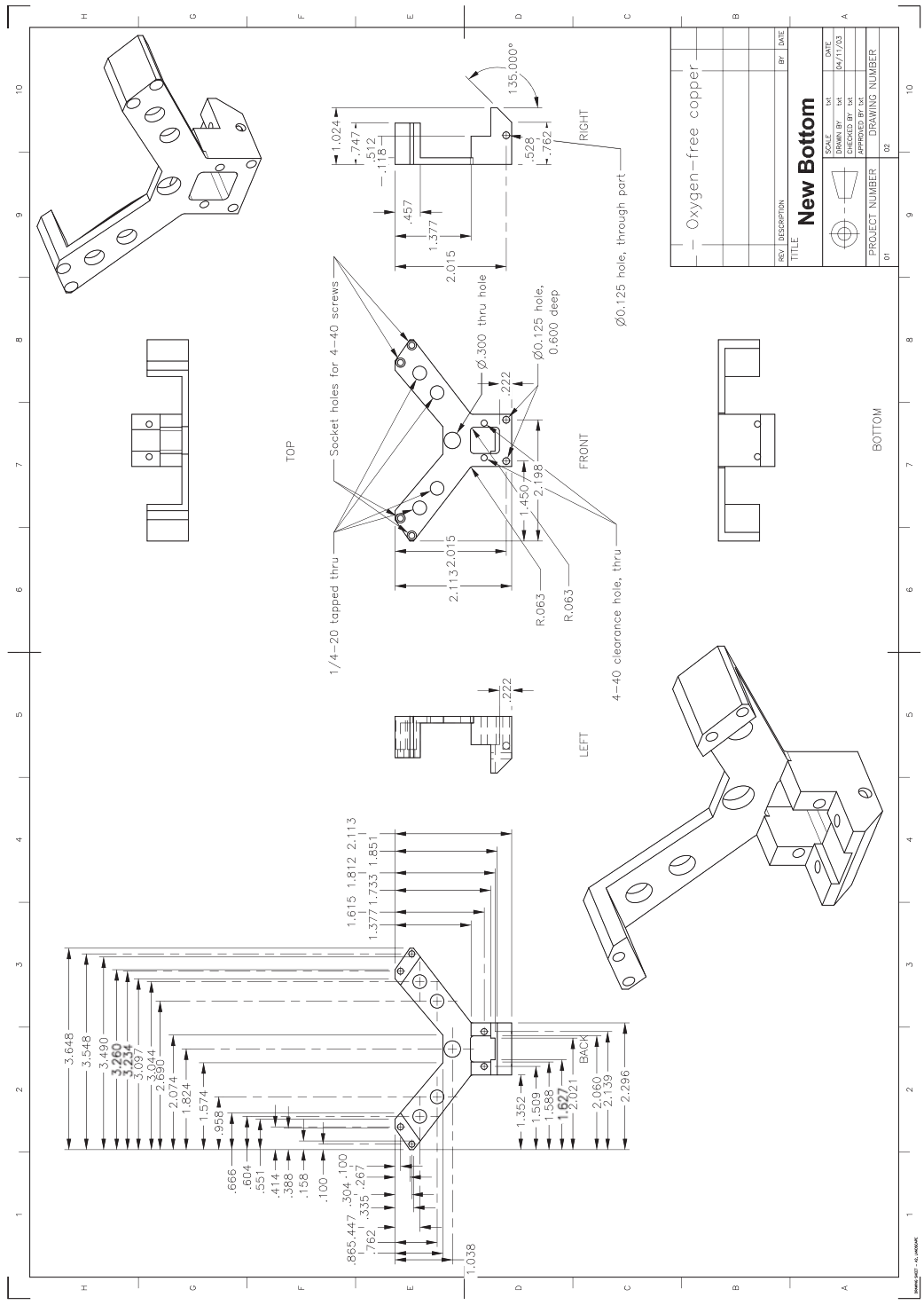

Figure C.2: The critical millitrap mounting piece. The winged structure mates with the main chamber (see Appendix A), and the bottom holes are plugged such that a closed path is made for liquid nitrogen circulation.

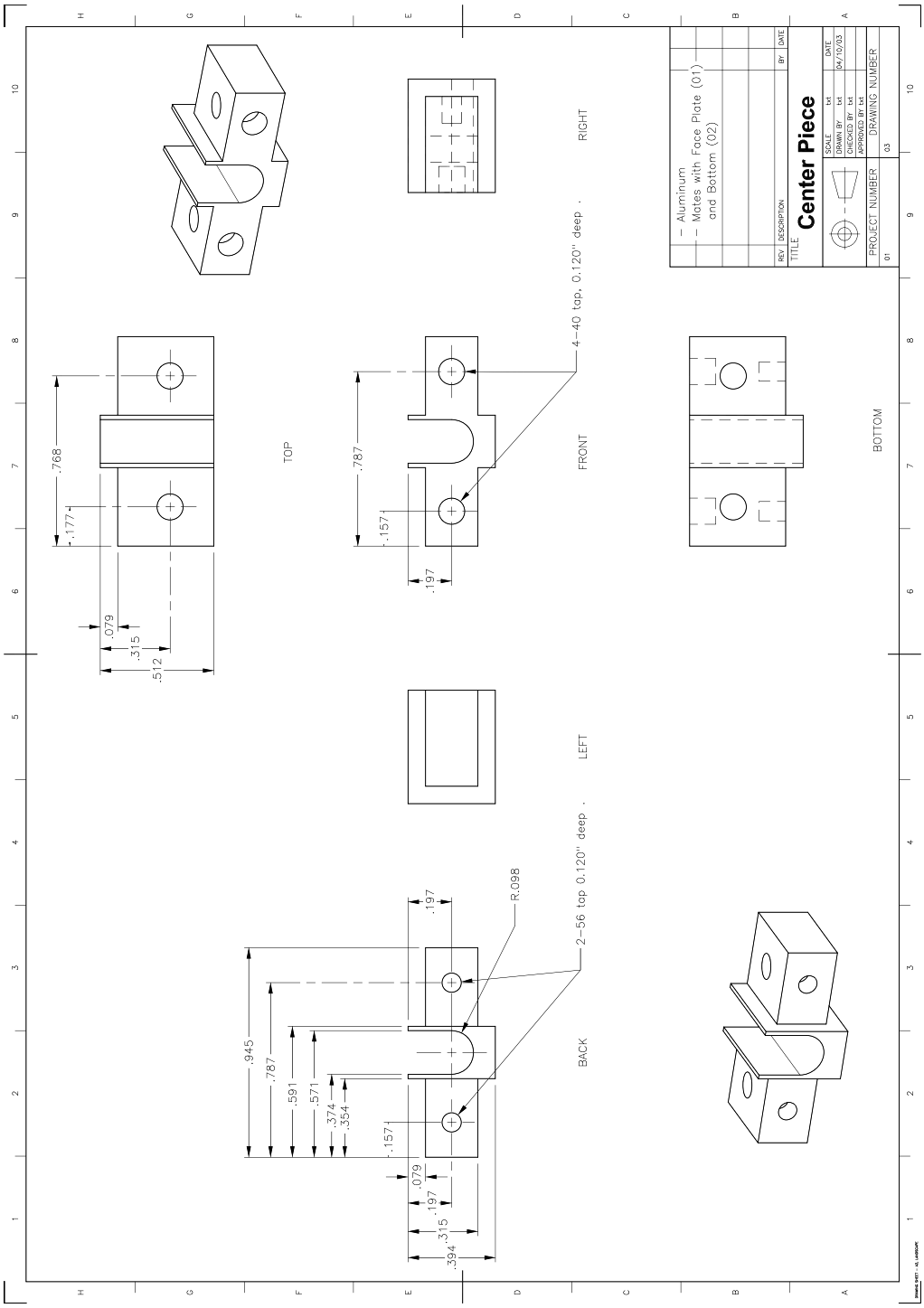

Figure C.3: The center piece, constructed out of aluminum and subsequently anodized.

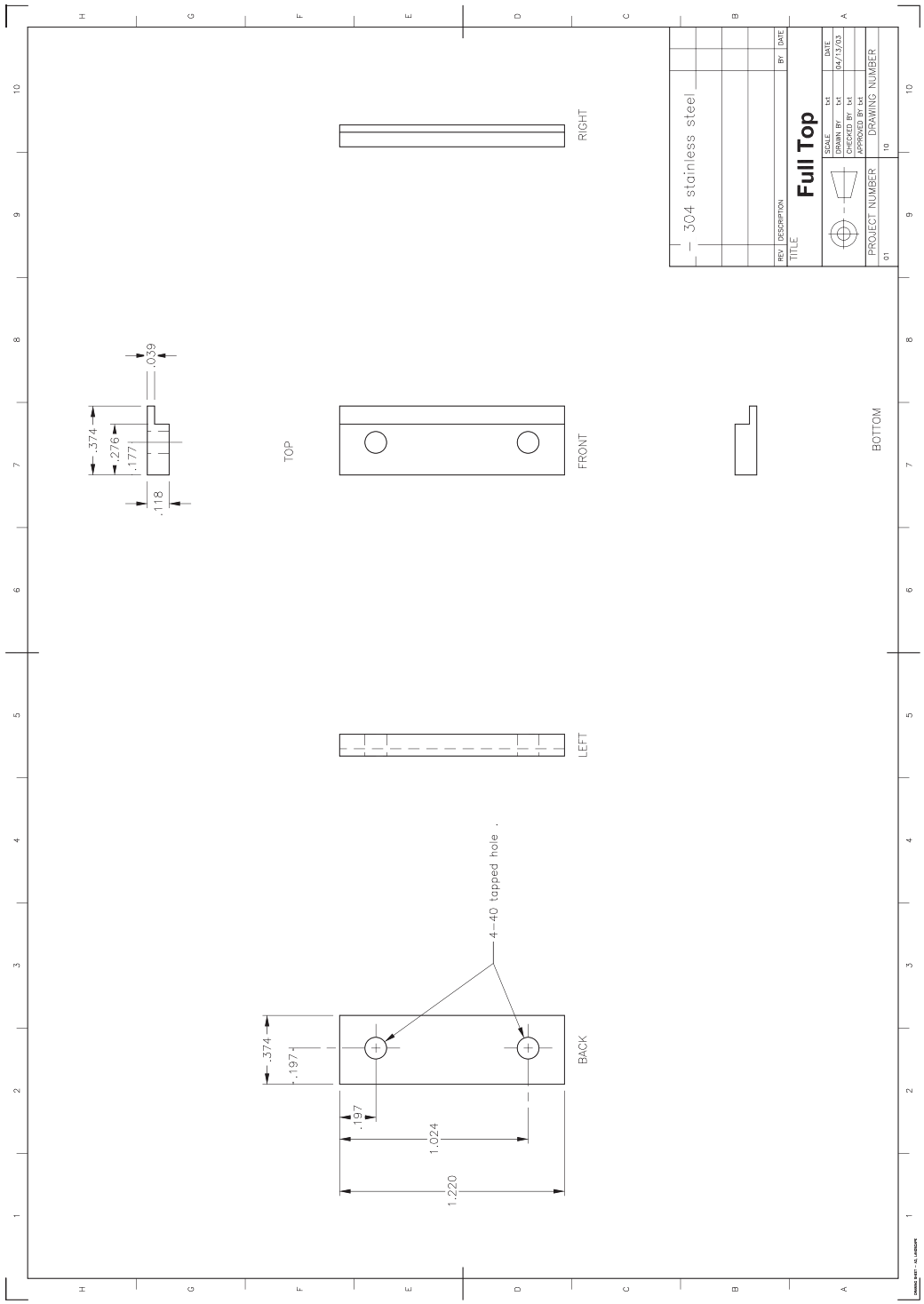

Figure C.4: The millitrap top bracket.

Appendix D

Designs for the Cavity Mounting Structure

This appendix includes the engineering schematics for the cavity mounting system.

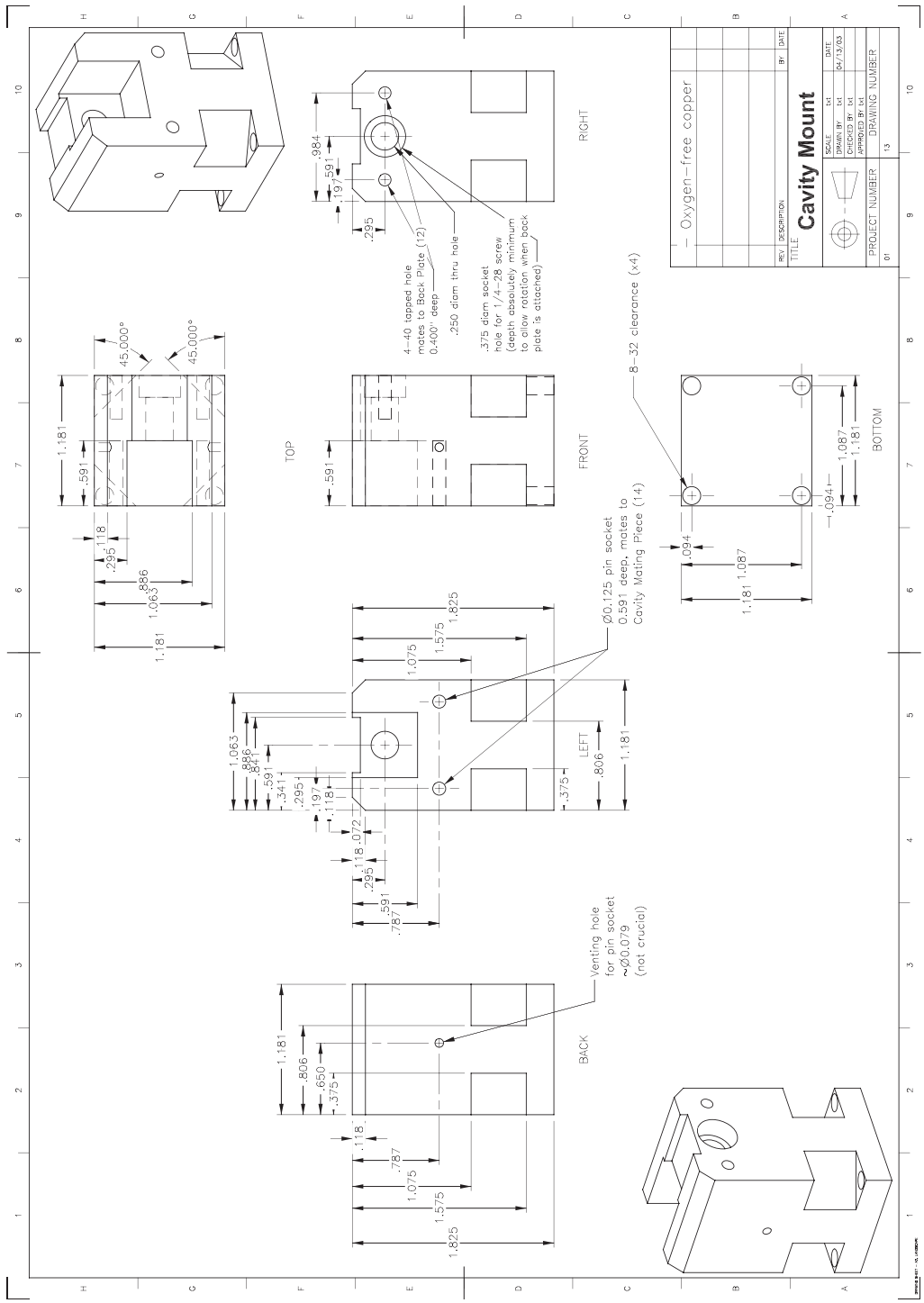

Figure D.1: The cavity mount.

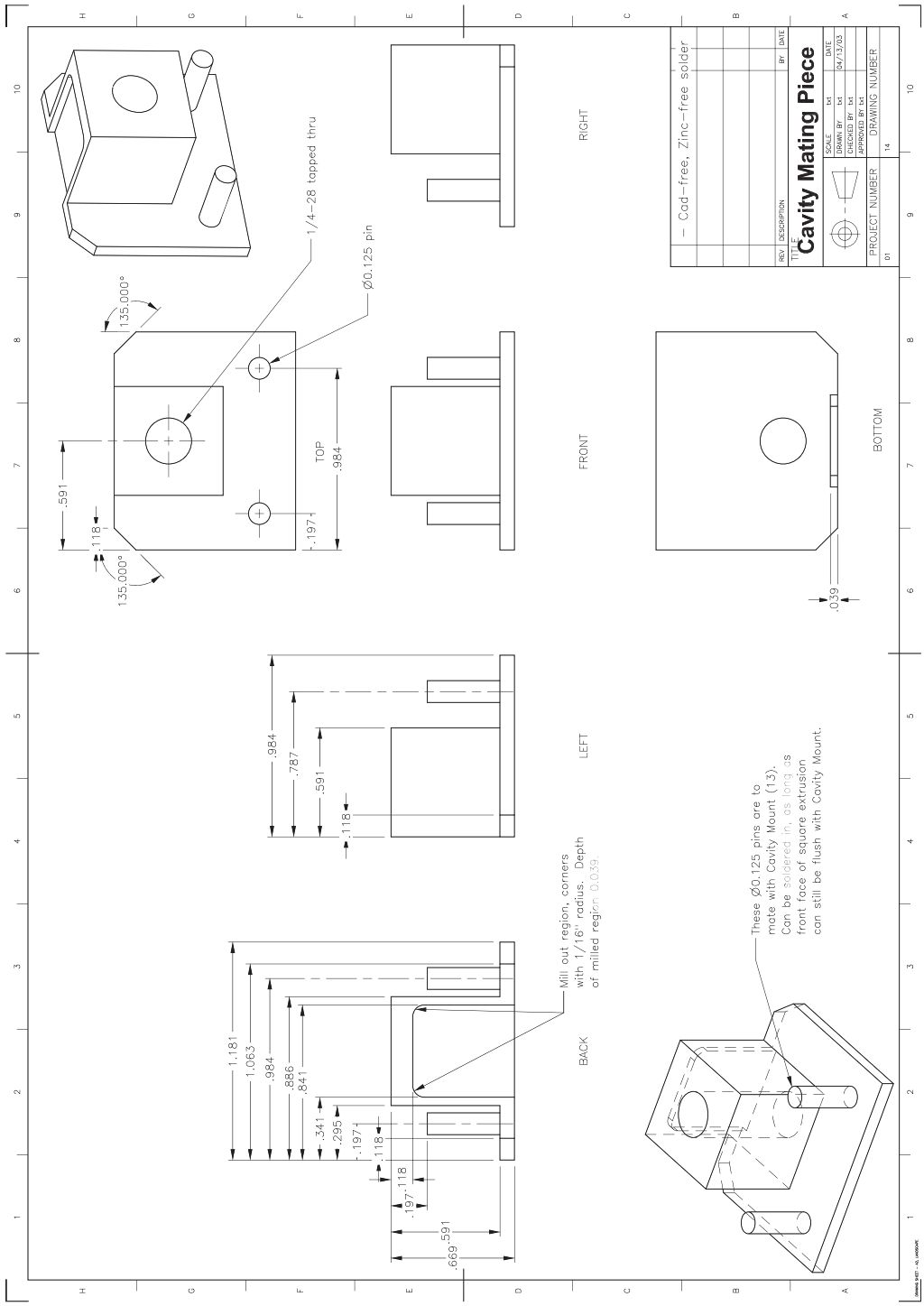

Figure D.2: The cavity mount mating piece, second mirror goes on here.

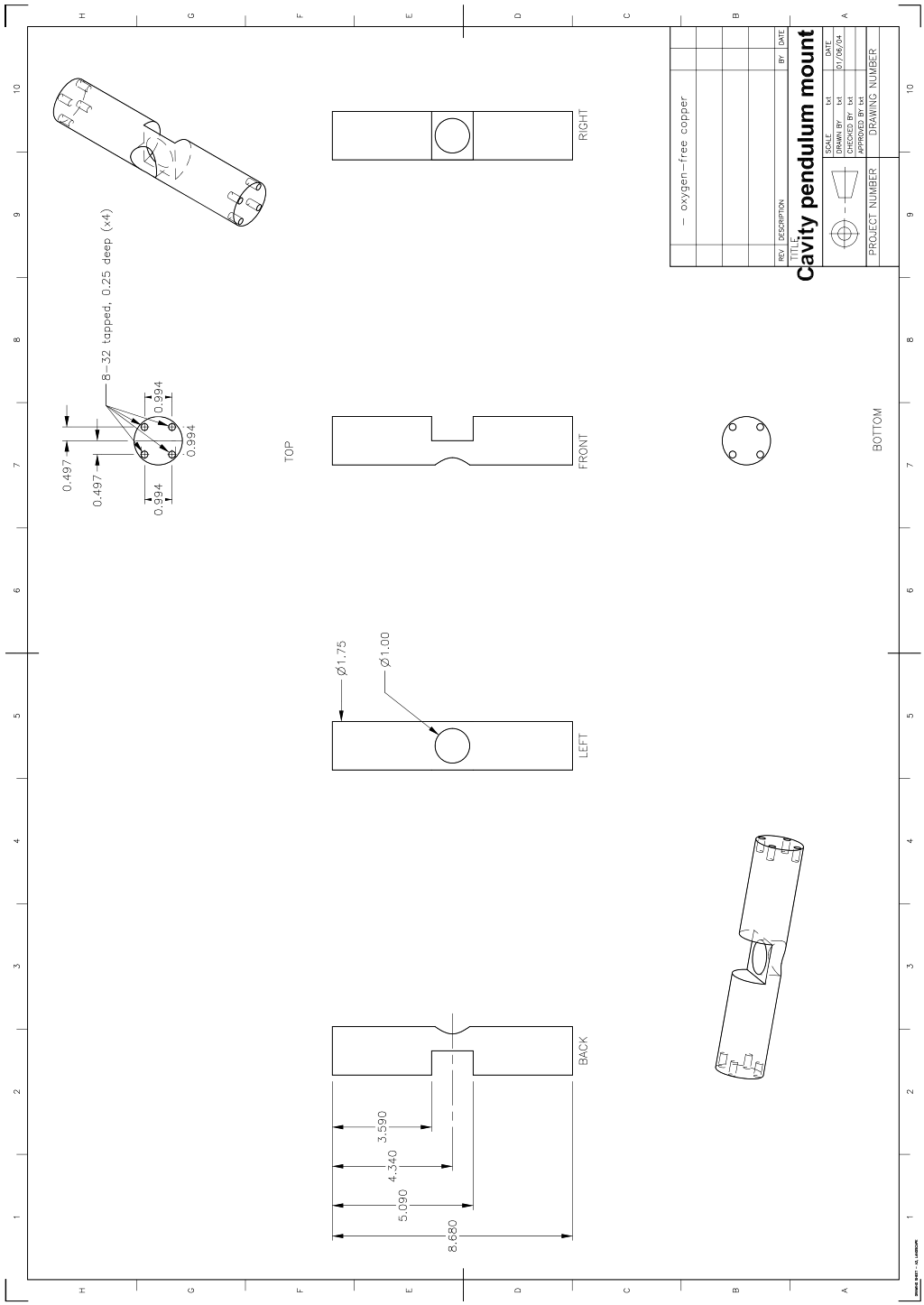

Figure D.3: The pendulum center piece.

Appendix E

Collimated, single-pass atom source from a pulsed alkali metal dispenser for laser-cooling experiments

This appendix includes the following paper:

- *K. L. Moore, T. P. Purdy, K. W. Murch, S. Leslie, S. Gupta, and D. M. Stamper-Kurn, "Collimated, single-pass atom source from a pulsed alkali metal dispenser for laser-cooling experiments," Rev. Sci. Instruments* ***76****, 023106 (2005)*

Collimated, single-pass atom source from a pulsed alkali metal dispenser for laser-cooling experiments

Kevin L. Moore,[a] Thomas P. Purdy, Kater W. Murch, Sabrina Leslie, Subhadeep Gupta, and Dan M. Stamper-Kurn
University of California, 366 LeConte Hall, Berkeley, California 94720

(Received 10 September 2004; accepted 9 November 2004; published online 10 January 2005)

We have developed an improved scheme for loading atoms into a magneto-optical trap (MOT) from a directed rubidium alkali metal dispenser in $<10^{-10}$ Torr ultrahigh vacuum conditions. A current-driven dispenser was surrounded with a cold absorbing "shroud" held at $\leqslant 0$ °C, pumping rubidium atoms not directed into the MOT. This nearly eliminates background atoms and reduces the detrimental rise in pressure normally associated with these devices. The system can be well-described as a current-controlled, rapidly switched, two-temperature thermal beam, and was used to load a MOT with 3×10^8 atoms. © *2005 American Institute of Physics.*
[DOI: 10.1063/1.1841852]

I. INTRODUCTION

The first step in the construction of an atomic physics experiment is obtaining an appropriate source of atoms. *Directed* sources of atoms have a long and storied history.[1] A thermal beam of atoms is easily obtained from an oven or other gas source, though this inevitably involves a differential pumping scheme, a $1/r^2$ decrease in atom flux with distance between the oven and the collection region, a mechanical shutter to quench the beam, and direct handling of a purified sample of the atom of interest. A Zeeman slower[2] can improve the flux of laser-cooled atoms from an oven, but suffers from the same drawbacks as an oven as well as the added complications of the magnetic design and the slowing beams. A multiply loaded magneto-optical trap (MOT) initially loaded from a vapor cell is a widely-used source for cold atom experiments,[3] but has the drawback of increased optical, electronic, and vacuum infrastructure. Light-induced atomic desorption (LIAD),[4] while not a collimated beam source, is an elegant technique which has recently been improved to yield very fast MOT loading rates.[5]

Alkali metal dispensers,[6] or "getters," have emerged as a useful alternative to these sources,[7,8] requiring only a modest electric current (<10 A) for their operation. The driving current rapidly heats the dispenser causing a reduction reaction, inducing the cm-scale devices to release an atomic vapor (rubidium, in our case) with a rapid turn-off time. The emitted atoms are quite hot, as the dispensers reach temperatures of 800 °C or more for typical current pulses.[7,8] The fraction of atoms capable of being captured by a typical MOT is quite small ($\approx10^{-5}$) due to the large temperatures reached, but the efficacy of the dispensers for direct loading is salvaged both by the large atom flux and their ability to be placed close to the MOT. Alkali metal dispensers are already used as sources for vapor cell MOTs (Refs. 9–11, for example), but in these cases the 800 °C atoms are cooled by the walls of the vapor cell so the loading rate into the MOT is increased.

Many ultracold atomic physics experiments demand base pressures of less than 10^{-10} Torr, particularly in the case of magnetic trapping of atoms for long periods of time. Getters have been used directly in an ultrahigh vacuum (UHV) ultracold atom experiment[12] and the atomic flux from a dispenser has been collimated to make an atom beam,[13] but to the best of the authors' knowledge no published work describes a system which attempts to control the output flux of the getter entirely in the UHV chamber.

The desire for a fast, simple, and efficient source of rubidium atoms with a minimal impact on UHV conditions led us to the development of a cold shroud for the rubidium dispenser and MOT system. The shroud acts as a pump for rubidium atoms released by the dispenser that are either (a) not directed towards the MOT, (b) of the wrong isotope, or (c) moving too quickly to be captured by the MOT. The dispenser-shroud system thus acts as a fast, compact, collimated atomic beam source with a minimized impact on UHV conditions.

This article discusses the performance of the getter-shroud system as well as the efficiency of loading atoms into a MOT from the direct flux of a dispenser. Importantly, our measurements characterizing the loading rate and equilibrium populations of a MOT indicate that direct loading of atoms from a getter is strikingly ineffective. In contrast, our measurements indicate that a secondary, lower temperature atomic source was also formed, contingent on operation of the getter, which was much more effective at loading a MOT at UHV conditions. Future getter-loaded, UHV experiments can be designed to make use of this tempered source in a more controlled manner.

II. EXPERIMENT

Our experiments are carried out in a stainless steel UHV chamber pumped to below 10^{-10} Torr (see Fig. 1). This

[a]Electronic mail: klmoore@socrates.berkeley.edu

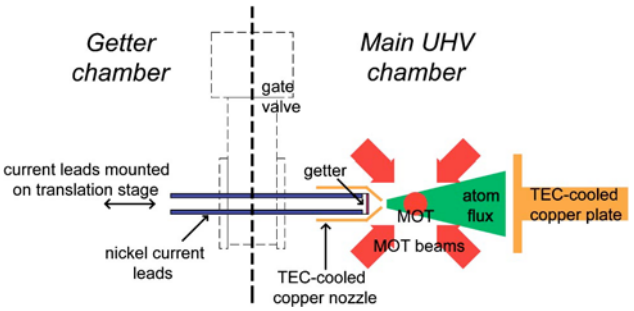

FIG. 1. (Color online) Essential elements of the getter and cold shroud system. The getter is brought within 1.2 in. of the MOT center, and with a driving current greater than 2.7 A it releases a hot rubidium vapor. When cold, the copper nozzle that surrounds the getter absorbs nearly all of the emitted rubidium atoms that are not directed through the open aperture towards the MOT. The MOT is loaded from the resultant atomic beam exiting the nozzle. The vast majority of emitted atoms are moving too quickly to be captured by the MOT, but are absorbed by the cold copper plate on the right. The shroud is comprised of the copper nozzle, the copper plate, and surrounding mechanical structure.

chamber is divided between a main chamber and a secondary "getter chamber," designed so as to allow defective or depleted getters to be replaced without exposure of the main UHV chamber to atmosphere. The getter is spot-welded to nickel rods and mounted on a hollow linear feedthrough[14] which provides six inches of travel. The current feedthrough also has a hollow interior (0.4 in. i.d. tube) and a 1.33 in. mini-flange port which accepts an electrical feedthrough to control the current through the getter. A single-rod current feedthrough is sufficient, as the return current path can be grounded to the chamber on the interior bellows of the linear motion feedthrough.

To prepare a new getter, the getter chamber is vented with dry nitrogen with the gate valve to the main chamber closed. It then takes less than 30 min to open the getter chamber, spot weld a new getter, and reseal the vacuum system. The "getter chamber" is then evacuated and undergoes a modest bakeout ($\approx$2 days), during which the dispenser is degassed as discussed by the authors of Ref. 7. We typically follow their procedure, although the alternate method advocated by Ref. 8 also provides a usable rubidium source.

When the gate valve is re-opened, pressures in the 10^{-10} Torr range are established in both the getter chamber and the main chamber. With the entry path though the gate valve clear, the dispenser can be translated to within 1.25 in. of the MOT center.

To ensure that rubidium atoms not captured by the MOT are pumped away, all line of sight from the dispenser to the room temperature UHV chamber is blocked by a nickel-plated cold copper shroud. As the shroud is cooled, the sticking probability for a rubidium atom (or any alkali metal) impacting the surface approaches unity. In theory this would protect all sensitive surfaces from the direct flux of atoms as well as preventing a room temperature background vapor of rubidium from permeating the chamber during an experiment. Figure 2 highlights the suppression of the background rubidium vapor with the cooling of the cold shroud; operating the getter while the shroud is at room temperature produces visible fluorescence throughout the chamber due to a

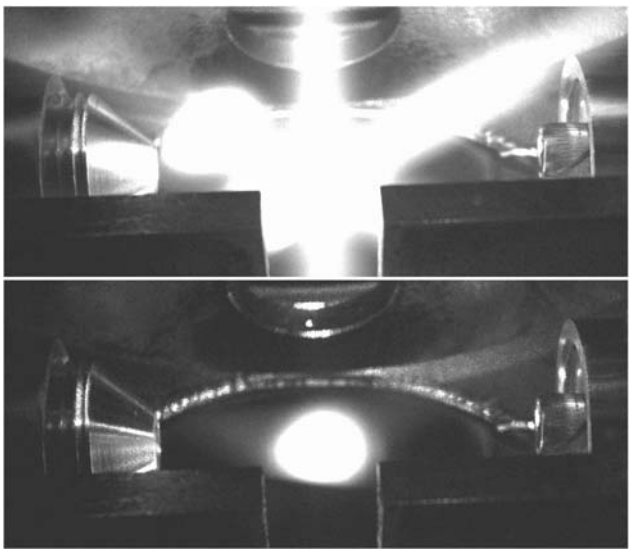

FIG. 2. Extinction of a background vapor and production of a single-pass atomic beam by low temperature shroud. The top image shows the fluorescence of the background rubidium atoms for a getter pulse of 10 A for 15 s at a shroud temperature of 21.5 °C. The bottom image is the fluorescence for an identical getter pulse and incident MOT beams, but instead the shroud is held at −30 °C. Note the sharp edges of the atom beam, as well as the disappearance of background fluorescence. In both images, the atom beam flows from left to right, consistent with the orientation of Fig. 1.

thermal rubidium vapor, while similar operation with a cold (−30 °C) shroud yields fluorescence only from a beam with line-of-sight access to the getter. The pressure spike associated with the dispenser heating, observable at 10^{-10} Torr with an ion gauge, is also reduced by nearly a factor of 2 with the cooling of the shroud, although not entirely eliminated because the dispenser and current leads outgas more than just rubidium at such high temperatures.

Atoms are collected in a MOT centered within the getter-emitted beam. The MOT is formed from 50 mW of total laser power split into four 0.75 in. diam beams, two of which are retroreflected. The quadrupole coils are placed outside the vacuum system, three inches from the center of the MOT, and are typically operated with axial field gradients of 20 G/cm. The MOT population was limited by the relatively small amount of light power per beam. The trends reported in this paper should scale directly with improvements in MOT loading.

III. RESULTS

Our pulsed atomic source should be evaluated under two criteria: first, that operating the source yields an atomic flux which is efficiently loaded into sizable MOTs, and, second, that the source can be quickly switched off to yield UHV conditions for subsequent experimentation (e.g., magnetic trapping and evaporation) of the laser-cooled atoms. We assessed the performance of our getter-shroud system under both criteria by measuring the loading rate and equilibrium population in MOTs formed either during or after the atomic source was pulsed: large MOTs formed during the getter pulse indicate efficient loading, while small MOTs formed seconds after the getter pulse indicate the desired suppression of the atomic flux when the source is turned off. Measure-

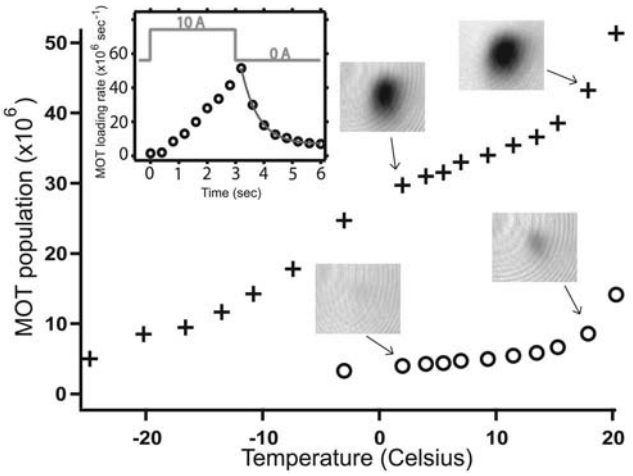

FIG. 3. MOT population as a function of shroud temperature. Crosses (+) denote a MOT loaded by a 10 A, 6 s pulse, circles (○) a MOT loaded from background atoms for 6 s with no getter pulse. Inset shows MOT loading rate as a function of time overlayed upon the current profile of a 3 s, 10 A getter pulse (the shroud temperature was 19 °C). The rapid quenching of the MOT loading rate upon cessation of the getter current has a decay time of 0.6 s.

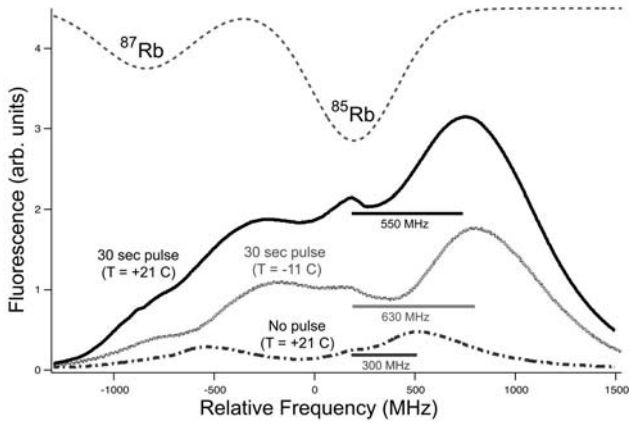

FIG. 4. Fluorescence spectra of atom flux in the MOT region. The probe laser beam was incident upon the atom flux at 45° to the center line of the the shroud nozzle. Dotted lines show absorption spectrum, inferred from an absorption signal generated in a reference rubidium vapor cell. Plotted are fluorescence curves when the shroud is at room temperature and at −11 °C, given a 30 s, 10 A current pulse to the getter. Also plotted is the background fluorescence in the MOT region with no getter pulse, clearly showing the sizable room temperature flux emitted from the room temperature shroud surface after a large layer of atoms have desorbed on the inner surface of the nozzle.

ments of MOT populations under both conditions (getter on/getter off) are shown in Fig. 3 as a function of the temperature of the shroud.

Several conclusions can be drawn from these data. First, at all temperatures of the shroud, the MOT populations formed through operating the getter are much higher than those collected from the background atomic flux, indicating that the getter-shroud system is indeed operating as a pulsed atomic beam source, as desired. Longer getter pulses make use of this high loading rate to reach equilibrium MOT populations of 3×10^8. Second, confirming the visual findings of Fig. 2, the cold shroud extinguishes the background rubidium vapor if it is operated at sufficiently low temperatures; below 0 °C, the MOTs formed from the background vapor were only barely detected by our optical absorption measurements. Further, the inset of Fig. 3 shows the rapid termination of the MOT loading rate upon extinguishing the getter current, satisfying the second stated criterion for the system.

While the getter-shroud system satisfies the stated criteria as an efficient, rapidly-switched atom source, these data exhibit some surprising features. The reason that the getter-loaded MOT depends so strongly on the shroud temperature, including an almost complete elimination of trapped atoms for the coldest temperatures, is not immediately obvious. The dispenser assembly has no mechanical contact with the shroud, meaning that the getter itself arrives at the same temperatures regardless of the temperature of the shroud. The small MOT populations for low shroud temperatures suggest that the direct atom flux from the getter is actually a rather poor source for a MOT. Our original intent was to utilize this shroud at or below −20 °C, but the reduced MOT population at lower temperatures forces a choice between rubidium background elimination and larger MOT populations. The optimum shroud temperature will likely vary for different experimental requirements.

In order to diagnose the thermal character of atoms emitted by the dispenser, a laser 45° to the atomic beam was scanned in frequency while fluorescence at the center of the MOT region was detected on a photodiode. This yields information about the velocity distribution of the emitted atoms, though the resultant spectrum is expected to be a convolution of many competing factors due to the large probe beam size (≈0.75 in. diameter), divergence of emitted atoms, optical pumping rates, and background fluorescence.

The fluorescence data (Fig. 4) show the effect of the cold shroud on the velocity distribution of the emitted atoms from a strong getter pulse (10 A, 30 s). For a shroud at room temperature the overall rubidium density in the MOT region is approximately twice that of a −11 °C shroud. At 21 °C the background rubidium vapor and the rubidium flux from the nozzle can be clearly distinguished, and the Doppler-shifted atoms show peak fluorescence at 550 MHz from the background vapor. At −11 °C, the background atoms are barely resolvable, and the Doppler-shifted atoms are now peaked at 630 MHz. Also plotted in Fig. 4 is the fluorescence curve for a room temperature (21 °C) shroud and no getter flux. In this case, the peak fluorescence in the MOT region is shifted by 300 MHz from the line center of the Doppler-broadened background rubidium spectrum. We believe this is caused by the flux of desorbing atoms from the shroud nozzle surface which acts as a directed, room-temperature background flux into the MOT region; we were only able to discern this fluorescence spectrum after an atypically large layer of rubidium had been deposited on the inner surface of the shroud nozzle.

These data explicitly demonstrates that the velocity distribution of the atomic flux through the nozzle and into the MOT region is significantly affected by the thermal state of the shroud. The strong dependence of the getter-loaded MOT population on shroud temperature in Fig. 3 is better under-

stood in this context, especially given the fact that a room temperature beam loads ≈10 times more atoms into a MOT than a 1000 K oven of the same number flux. The most likely explanation for the modification of the atom flux is that a large fraction of the atomic flux from the getter is impingent upon the cold nozzle used to collimate the remaining flux. If the surface has a substantial probability of reflecting and *thermalizing* these atoms, then a flux seemingly colder than the getter-only flux seen at −11 °C will be emitted because the emitted atoms will be a mixture of hot getter-emitted atoms and cooler reflected atoms. The thermalization of getter-emitted atoms with surrounding walls has been previously observed.[13] The sum of these two fluxes yields the reduced Doppler shift seen in the room temperature data in Fig. 4. We found that after a few weeks of normal operation of the getter the desorbing flux would then persist for several days.

IV. DISCUSSION

While the dispenser-shroud system has proven itself to be potentially useful for ultracold atomic experiments, there are some drawbacks. We tried many different avenues for continuous operation in an attempt to maximize MOT population and minimize the experiment repetition time. If the getter is pulsed too frequently (<20 s separation between 3 s, 10 A pulses) the pressure in the chamber rises to a steady state above the minimum base pressure. While we believe this to be an improvement over bare operation of a dispenser in UHV, we had hoped to reduce this repetition time further. However, even with the coldest shrouds that the TEC system could effect we were unable to execute an experimental cycle of less than 20 s.

Second, rubidium adsorbed on the shroud will be released into the UHV if the shroud is allowed to warm up. If one is to prevent this substantial gas load from interfering with in-vacuum equipment (such as ion pumps or high-finesse mirrors), the cooling of the shroud must be made fail safe. Furthermore, one would not be able to bake the shroud in UHV. Thus contamination of the UHV chamber would be correctable only by selective baking or by thoroughly cleaning the chamber. This disadvantage belies the purpose of the getter as an easily-exchanged UHV atom source.

Drawbacks aside, several improvements to our design could be made which would make the system a useful tool in many instances. First, the aperture on the nozzle could be widened to allow a larger flux into the MOT. The aperture is currently 0.25 in. in diameter and appears to "choke" the MOT at lower temperatures because the beam is only shining into a fraction of the MOT cross section. A larger aperture would increase the flux as the square of the aperture diameter, allowing the maximum getter-loaded population number to be reached in less time with a reduced impact on the pressure.

Another improvement would be the addition of a "shadow" for the getter. This would likely take the form of a metal piece which would obscure the getter slit from direct line of sight to the center of the MOT. This should drastically reduce the losses due to MOT atoms colliding with fast Rb atoms, allowing for a larger final MOT population.

Finally, given our understanding of the fluorescence spectrum in Fig. 4, one could construct a system which would utilize the secondary room temperature beam generated by the rubidium-coated surfaces of the shroud. A miniature "oven," operated in the main UHV chamber, could surround a dispenser that purposefully directs its atomic flux towards the inner walls of the oven. Atoms emitted from the getter would be tempered by the inner surface of the oven, and these thermalized atoms would then be allowed to escape through a collimated aperture to efficiently load a closely situated MOT. Cold baffles would then be placed behind the MOT to pump away the atoms which are not captured by the MOT. During experimental operation the oven could be held at or slightly above room temperature to increase atom yield and prevent a surface layer of atoms from forming. When the experimental system is not in operation the miniature oven could be heated further to release any remaining adsorbed atoms onto the cold baffles.

ACKNOWLEDGMENTS

The authors thank Stefan Schmid, Mike Grobis, and Dave Murai for their technical assistance and advice. The authors effort was sponsored by the Defense Advanced Research Projects Agency (DARPA) and Air Force Laboratory, Air Force Materiel Command, USAF, under Contract No. F30602-01-2-0524, the National Science Foundation under Grant No. 0130414, the Sloan Foundation, the David and Lucile Packard Foundation, and the University of California. K.L.M. acknowledges support from the National Science Foundation. S.G. acknowledges support from the Miller Institute for Basic Research in Science.

[1] N. F. Ramsey, *Molecular Beams*, reprint ed. (Oxford University Press, Oxford, 1997).
[2] W. D. Phillips and H. Metcalf, Phys. Rev. Lett. **48**, 596 (1982).
[3] C. J. Myatt *et al.*, Opt. Lett. **21**, 290 (1996).
[4] B. P. Anderson and M. A. Kasevich, Phys. Rev. A **64**, 023404 (2001).
[5] S. N. Atutov *et al.*, Phys. Rev. A **67**, 053401 (2003).
[6] Manufactured by SAES Getters USA Inc.
[7] J. Fortagh, A. Grossman, T. W. Hansch, and C. Zimmermann, J. Appl. Phys. **84**, 6499 (1998).
[8] U. D. Rapol, A. Wasan, and V. Natarajan, Phys. Rev. A **64**, 023402 (2001).
[9] H. J. Lewandowski, Ph.D. thesis, University of Colorado, 2002.
[10] M. R. Matthews *et al.*, Phys. Rev. Lett. **81**, 243 (1998).
[11] C. Wieman, G. Flowers, and S. Gilbert, Am. J. Phys. **63**, 317 (1995).
[12] H. Ott *et al.*, Phys. Rev. Lett. **87**, 230401 (2001).
[13] T. M. Roach and D. Henclewood, J. Vac. Sci. Technol. A **22**, 2384 (2004).
[14] Manufactured by Thermionics Vacuum Products, part number FLMH-275-50-6. Inclusion of this item is not an endorsement; we expect that devices from other manufacturers would behave in a similar fashion.

Appendix F

Bose-Einstein condensation in a mm-scale Ioffe Pritchard trap

This appendix includes the following paper:

- *K. L. Moore, T. P. Purdy, K. W. Murch, K. R. Brown, K. Dani, S. Gupta, and D. M. Stamper-Kurn, "Bose-Einstein condensation in a mm-scale Ioffe-Pritchard trap," Applied Physics B* ***82****, 533-538 (2006)*

Bose-Einstein condensation in a mm-scale Ioffe-Pritchard trap

Kevin L. Moore,* Thomas P. Purdy, Kater W. Murch, Kenneth R. Brown, Keshav Dani, Subhadeep Gupta, and Dan M. Stamper-Kurn
Department of Physics, University of California, 366 LeConte Hall #7300, Berkeley, CA 94720
(Dated: March 31, 2005)

We have constructed a mm-scale Ioffe-Pritchard trap capable of providing axial field curvature of 7800 G/cm^2 with only 10.5 Amperes of driving current. Our novel fabrication method involving electromagnetic coils formed of hard anodized aluminum strips is compatible with ultra-high vacuum conditions, as demonstrated by our using the trap to produce Bose-Einstein condensates of 10^6 ^{87}Rb atoms. The strong axial curvature gives access to a number of experimentally interesting configurations such as tightly confining prolate, nearly isotropic, and oblate spheroidal traps, as well as traps with variable tilt angles with respect to the nominal axial direction.

PACS numbers: 03.75.Nt, 32.80.Pj, 05.30.Jp

Magnetic traps have become a staple of ultracold atomic physics. As such, innovations in magnetic trapping techniques have consistently led to new experimental breakthroughs. For example, the invention of the time-orbiting-potential (TOP) trap to stem Majorana losses in spherical quadrupole traps led to the first gaseous Bose-Einstein condensates (BECs) [1]. The cloverleaf trap [2], the QUIC trap [3], and other electro- and permanent magnet configurations allowed for stable confinement of large BECs with DC fields and variable aspect ratios; these capabilities led, for example, to precise tests of mean-field theories [4], observations of quasi-condensates in reduced dimensions [5], and studies of long-lived hyperfine coherences in two-component gases [6]. The rapidly-developing magnetic-trapping technology of atom chips now provides new capabilities for manipulating ultracold atoms and studying their properties (e.g. coherence of condensates in a waveguide [7], the decay of doubly-charged vortices in a BEC [8], etc.).

A typical configuation for magnetic trapping with DC magnetic fields is the Ioffe-Pritchard (IP) trap [9]. Near the trap center — at distances small compared to the size of or distance to the magnets used to generate the trapping fields — an IP trap is characterized by three quantities: the axial bias magnetic field B_0, the radial quadrupole field gradient B'_ρ, and the axial field curvature B''_z. The magnitudes of these parameters scale as I/d, I/d^2 and I/d^3, respectively, where I is the total current carried in the wire(s) (or magnetization of ferromagnets), and d is their characteristic length scale or distance from the location of the magnetic trap center. Both because of this scaling, and because the effective radial curvature can be greatly increased by lowering the bias field B_0, the limitation to the confinement strength of an IP trap comes typically from the maximum axial curvature which can be attained.

As indicated by the I/d^3 scaling of the axial curvature, strategies for increasing the confinement of an IP trap involve both increasing the current in the coils and decreasing the characteristic size scale of the trap. Magnetic traps used in most ultracold atom experiments have been constructed on one of two different length scales. Centimeter (inch) scale traps, which provide superior optical access, utilize currents of 1000's of Amperes, typically distributed as smaller currents in each of several turns of wire. The highest currents sustainable in such traps, limited by resistive heating, restrict axial field curvatures to the neighborhood of 100 G/cm^2.

Alternatively, magnetic confinement can be provided with modest currents by reducing the field-producing wires and their distance to the ultracold atoms to microscopic sizes. This strategy has been carried out effectively with surface microtraps [10–12], resulting in versatile ultracold atomic experiments. The typical size scale for these microfabricated magnetic traps is $\sim$100 μm, and typically only 1 A of current is required to produce IP traps with field curvatures in excess of 10^4 G/cm^2 [11, 13]. Microtraps are not ideally suited for all experimental endeavors, however, as the atomic cloud is trapped $\sim$100 μm or less from the planar surface.

In this article we describe the design, construction, operation, and performance of a millimeter-scale, $\sim$10 A (or $\sim$ 100 Ampere-turns) magnetic trap which bridges the two aforementioned regimes. This "millitrap" utilizes a novel fabrication scheme which allows for the production of axial field curvatures of over 7800 G/cm^2 and is shown to be compatible with experimental requirements for the creation of large BECs. We demonstrate that this trap, owing to its high axial field curvature, allows for a wide range of trapping geometries, ranging from the typical prolate spheroidal to the more unusual oblate spheroidal configuration. Further, we describe a modification of the IP trapping fields which allows for traps with a variable tilt angle with respect to the nominal axial direction, a capability which is compatible with excitation of the "scissors mode" [14], the creation of vortices [15, 16] or other studies of superfluid flow [17, 18] in a BEC. The trap is also suitable for loading and trapping an ultracold atomic gas inside a high-finesse cavity formed by conventional mm-scale mirrors [19–21](or near other mm-scale

*Electronic address: klmoore@socrates.berkeley.edu

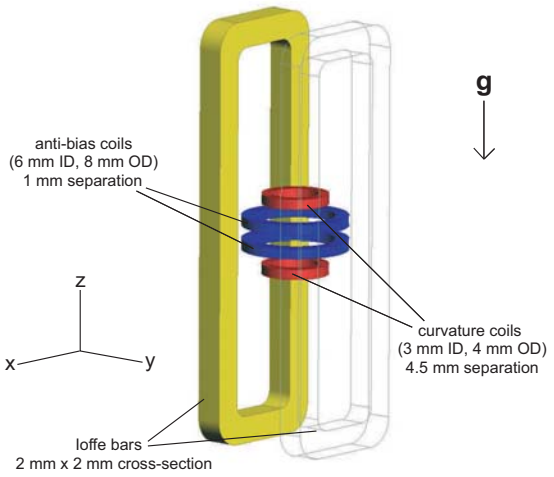

FIG. 1: Sketch of the mm-scale IP trap. The primary curvature coils (red), the anti-bias coils (blue), and the gradient coils (yellow) are depicted in this diagram as solid bodies, but are in actuality multiple turns of wire with protruding leads. For clarity the coil leads have been omitted and the nearest gradient coil is shown as transparent. *Higher resolution version of figures at http://physics.berkeley.edu/research/ultracold.*

objects).

The winding pattern of the millitrap is similar to that of inch-scale IP traps (see Figs. 1 and 2). The axial field is shaped by two pairs of coaxial coils, with parallel currents in each pair of coils but opposite currents in each of the two pairs. The small diameter coils ("curvature coils") are positioned to generate the maximum possible curvature given their diameter. The larger diameter coils ("anti-bias coils") allow for near cancelation of the large bias field produced by the curvature coils at the trap center, while their small axial separation allows for a slight increase (about 15 %) in the total axial curvature. Finally, two elongated rectangular coils ("gradient coils"), run antiparallel currents to produce a radial quadrupole field. The dimensions of various coils were chosen to maximize axial curvature while allowing for a 3 mm diameter cylindrical clearance along the trap axis (for the later accommodation of mirrors for a Fabry–Perot cavity), and a 1 mm clearance along the radial directions for the purpose of imaging. Further details on the positioning and cross sectional area of the coils are shown in Table I.

To maximize the current density while avoiding large input currents and uncontrolled magnetic fields from current leads, multi-turn coils (with total cross sections on the order of 1 mm^2) were used. The maximum current density attainable in coils fabricated by various methods is limited by the steady state temperature of the coils, due to the tendency of the coil resistance to rise with temperature. We found that, for all implementations, there is a threshold at which no more current can be added to a coil without the resistance increasing exponentially from overheating. Thus, in order to minimize resistive heating and maximize heat dissipation, it is desirous to choose a fabrication method which allows for the cross-sectional area to be efficiently packed with current carrying conductor rather than electrical (and typically thermal) insulation.

Guided by these criteria, we chose to form electromagnetic coils from multiple turns of hard-anodized pure aluminum foil strips. The assembly procedure is illustrated in Fig. 2. Shear-cut strips of aluminum foil were cleaned and then hard anodized in sulfuric acid after smoothing their jagged edges with lubricated fine grit sandpaper. The thickness of the insulating Al_2O_3 layer (on the order of microns) was controlled by varying the duration of the anodization, and chosen to be thick enough to reliably prevent current shorts between turns of the coil but thin enough to allow the coils to be wound without fracture. Coils were then wound on Teflon mandrels with a UHV-compatible, thermally-conductive epoxy applied between turns. The epoxy was set by baking the coil and mandrel at 150°C for two hours, after which the coil was removed and then tested for electrical shorts through both DC resistance measurements and AC magnetic field measurements.

The coils were then inserted into a compound mounting and heat-sinking structure and secured by epoxy (curvature and antibias coils) or by pressure (gradient coils). Portions of the mount in contact with the coils were formed from hard-anodized aluminum. Current connections to the coil were formed by removing oxide layers from the leads and then clamping them tightly between two pieces of copper. Finally, the trap and mounting structure was installed in a UHV vacuum chamber, with current connection made through polyimide-insulated copper wires to a set of 20 A vacuum current feedthroughs. The mounting structure also contains two hollow channels for circulation of liquid nitrogen. Operating the magnetic trap at liquid nitrogen temperatures lowers the resistance of the aluminum coils by a factor of four compared to that at room temperature, allowing higher current densities to be maintained. Following a bakeout of the millitrap at a temperature of 250°C, lifetimes of over 100 s were observed for atoms trapped in the millitrap, demonstrating the vacuum compatibility of all materials used in its construction.

To provide the most flexibility in operating the millitrap, separate electrically-floating power supplies were used for each coil. Also included in the electrical setup were a set of inductor-capacitor filters and an interlock system to protect the millitrap from overheating. Electrical characterization of the millitrap following the vacuum bakeout revealed several undesired low-resistance (several Ohm) connections between different coils, indicating electrical connections through the common mounting structure. These inter-coil connections should have no effect since independent supplies are used for each coil. The possible presence of undesired intra-coil connections,

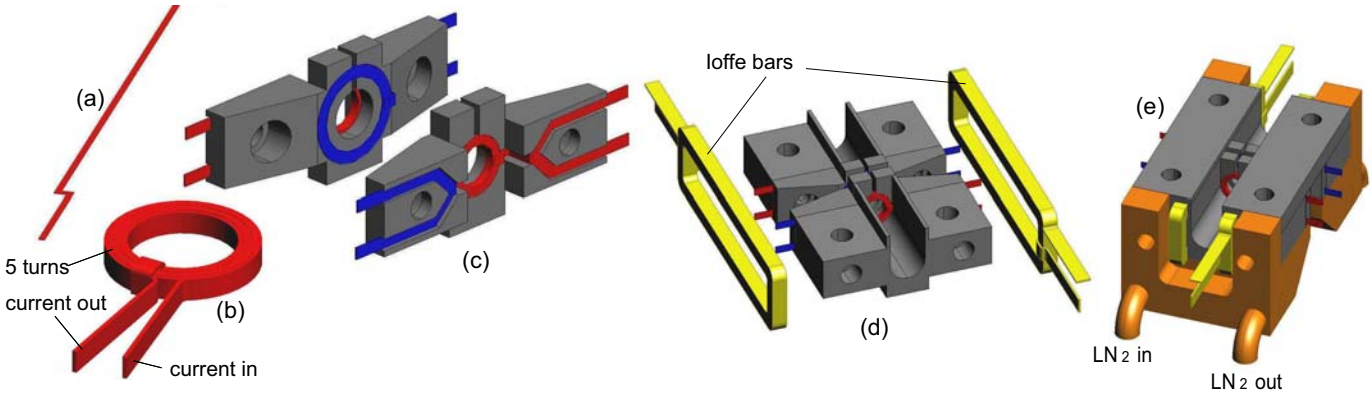

FIG. 2: Sketch of the assembly procedure and part integration. (a) Aluminum strips were cut with a z-shaped pattern to allow for the extraction of the interior current channel after the coil is wound. (b) A curvature coil with input and output current leads. (c) Curvature coils (red) and anti-bias coils (blue) were epoxied into anodized aluminum (grey) faceplates; current leads protrude from sides. (d) The faceplates were attached to an anodized aluminum mount which allows the gradient coils (yellow) to slide over the assembly. (e) A top fixture plate holds the mount in place by bolting into a copper mount (orange) below. A closed path inside the copper piece allows liquid nitrogen to be circulated.

TABLE I: Parameters for aluminum coil windings.

Coil	Inner Diam.	Outer Diam.	Foil thickness	Width	Cross-section	No. turns	Heat generated @ 10 A
curvature	3 mm	4 mm	0.006 in.	1 mm	0.5 mm^2	5	2 Watts
anti-bias	6 mm	8 mm	0.008 in.	0.75 mm	0.75 mm^2	4	2 Watts
gradient	N/A	N/A	0.008 in.	2 mm	4 mm^2	9	10 Watts

e.g. connections between turns on the multiple-turn coils, was tested by measuring parameters of magnetic traps formed with varying currents in each of the curvature, anti-bias, and gradient coils. No clear evidence for such flaws was obtained.

Cold atoms were loaded into the millitrap by optically cooling and trapping atoms in one portion of the UHV chamber, and then magnetically transporting them to the millitrap region. This multi-stage experimental procedure is depicted in Fig. 3. In a "loading region" which is displaced 3 inches horizontally from the millitrap, a 5×10^9 atom MOT was loaded from a Zeeman slowed beam of ^{87}Rb. About 2×10^9 atoms were trapped in the $|F = 1, m_F = -1\rangle$ magnetic sublevel by a spherical quadrupole magnetic trap with an axial gradient of 200 G/cm. The atoms were then transported using two sets of stationary anti-helmholtz coil pairs external to the chamber (similar to Ref. [22]), one of which is centered at the "loading region" and which is used for the initial spherical quadrupole trap and the other centered at the millitrap. As the two anti-helmholtz coil pairs overlap each other, the magnetically-trapped cloud was easily transported between the two coil centers by varying the currents in the two quadrupole coil pairs. During this transport, the atomic cloud was cooled by RF evaporation to reduce the cloud size to about 400 μm before passing the atoms through the 1 mm gap between the millitrap anti-bias coils.

Transfer of the atoms from the external-coil-based spherical quadrupole trap to the IP trap was accomplished in two stages of "handshaking." First, atoms were transferred to a spherical quadrupole trap formed by two of the six millitrap coils (a curvature coil and an opposing anti-bias coil); at 2 A running through each of these coils, a quadrupole trap with 150 G/cm axial gradient was produced, nearly matching the field strength generated by 400 A of current running through the external quadrupole coils. The spherical quadrupole trap was then suddenly (within 100 μs) replaced with the IP millitrap. This sudden quadrupole-to-IP transfer caused 25% (or less) of the atoms to be lost. RF evaporative cooling was then performed in a prolate IP trap, with trapping frequencies of $(\omega_x, \omega_y, \omega_z) = 2\pi \times (151, 138, 52)$ Hz (axes oriented as in Fig. 1), yielding atomic clouds near or below the BEC transition temperature (about 300 nK for our system). The transition temperature was reached with 2.5×10^6 atoms, and nearly pure condensates of 1×10^6 atoms produced upon further cooling.

The strongest confinement provided by the millitrap depends on whether such confinement is provided for long or for short trapping times. For example, up to about 7 A of current can be maintained in the curvature and anti-bias coils on a steady-state basis. Coils were safely operated at higher currents, up to about 11 A, although we found that after about 100 ms, the resistive heating of the coils led to increased outgassing which worsened the vacuum conditions in the millitrap region. The axial curvature provided under these conditions was mea-

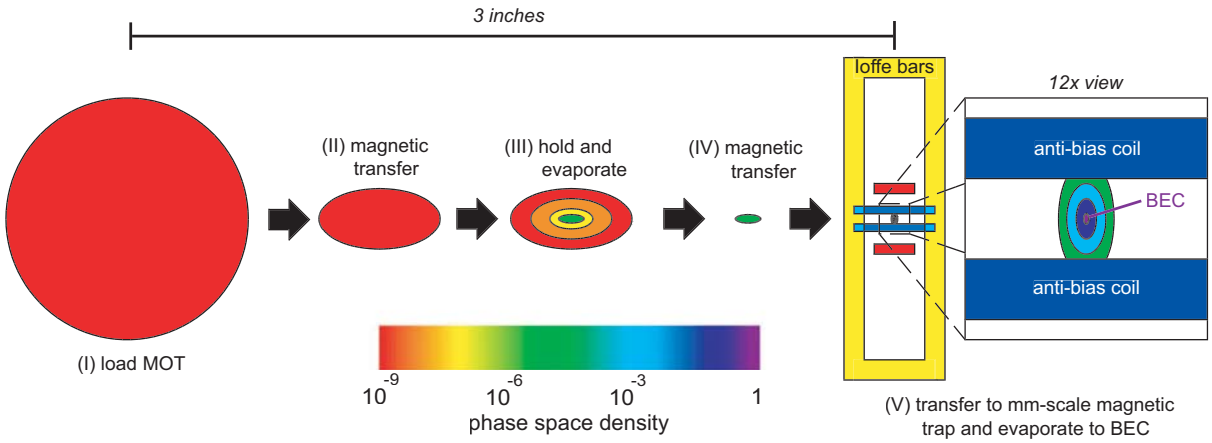

FIG. 3: Sketch of experimental sequence. (I) Atoms are loaded into the MOT and subsequently trapped in a spherical quadrupole trap. (II) The atoms are then transferred 1.75 inches towards the mm-scale IP trap and (III) evaporated to a phase space density of $\Gamma \sim 10^{-5}$. (IV) The cloud is magnetically transferred into the IP trap and (V) captured by a curvature coil and an anti-bias coil in a spherical quadrupole trap. The full millitrap is then turned on and the atoms are confined in the IP field with a 2 G bias field. The cloud is then further evaporated, forming a pure BEC of 1 million atoms.

sured in-situ using the trapped atoms as a probe, both by measuring the axial oscillation frequency of the trapped cloud, as well as by measuring the axial displacement of the cloud due to the application of a known axial field gradient. From these measurements, we determine that steady-state axial curvatures of 5300 G/cm^2 (7 A setting) and brief confinement with 7800 G/cm^2 (10.5 A setting) can be reached. Gradient coils are operated at a maximum of 11 A, yielding radial gradients of 220 G/cm.

One unexpected feature of this strong IP trap is a remarkably high efficiency of RF evaporation. This efficiency can be quantified by comparing the factor gained in phase space density Γ through the evaporative cooling loss of a given factor in atom number N, obtaining, e.g. a figure of merit $f = -d\ln\Gamma/d\ln N$, with Γ and N parameterized along some evaporation trajectory. Typical figures of merit cited in the literature for evaporation from IP traps are $f = 2$ to $f = 3$ [23, 24]. In our mm-scale IP trap, a factor of over 10^5 in phase space density is efficiently gained by evaporative cooling to the Bose-Einstein condensation transition temperature with an overall figure of merit of $f = 4.5$.

To account for this high efficiency, we note that the IP trap, aside from being strongly confining and thus compressing atomic clouds to high collision rates, is also nearly isotropic. We suspect that the condition of near isotropy improves the efficiency of evaporative cooling relative to that in the typically-used anisotropic traps since high-energy atoms produced collisionally in the gas can easily escape the center of the cloud in *any direction*, and thereby reach the trap boundary established by the applied RF radiation. In contrast, in a cigar-shaped cloud with high aspect ratio, the large axial collisional depth can prevent the escape of all high-energy atoms except those travelling nearly purely in the radial direction. Further, we note that high evaporation efficiency is obtained in our trap in spite of the vertical orientation of the axial direction; in contrast, IP traps with weaker axial confinement are rarely oriented in this manner so as to avoid the onset of lower dimensional evaporation due to gravitational sag [24, 25].

We have investigated several new features which are afforded by the large axial curvature in our trap. For instance, considering the generic magnetic field configuration of an IP trap and expanding about the minimum of the magnetic field, an effective radial curvature is obtained as $B''_\rho = {B'_\rho}^2/B_0 - B''_z/2$. The dependence of the radial trap strength on the applied bias field B_0 offers a simple means of varying the aspect ratio of the trap arbitrarily, ranging from prolate ($B''_z > B''_\rho$) to near-isotropic ($B''_z \simeq B''_\rho$) to oblate ($B''_z < B''_\rho$) geometries. While experiments using IP traps have typically employed prolate or near-isotropic geometries, the oblate geometry has been avoided since the very weak confinement afforded by such traps (limited to below the already weak axial confinement), makes it difficult to compensate for gravitational sag and stray magnetic fields. Thus, by greatly boosting the typical axial confinement strength, our trap gives more convenient access to oblate DC magnetic traps, with advantages for the study of two-dimensional [26–28] and/or rotating condensates.

Fig. 4 shows the range of trapping geometries accessed by our millitrap. After evaporatively cooling a thermal gas to a temperature of about 500 nK, the bias field B_0 was ramped to values ranging from 2 G to 18 G while holding the axial curvature at $B''_z \simeq 4000$ G/cm^2 and radial gradient at $B'_\rho = 205$ G/cm. We then displaced the cloud slightly in this new trap configuration, and recorded the harmonic motion of the trapped cloud to determine trap frequencies along three orthogonal directions. For this purpose, absorption imaging was employed along either of two imaging axes — one through

the 3 mm vertical aperture along the vertical trap axis, and the other along the horizontal $\hat{y}$ direction through the 1 mm gap between the anti-bias coils.

These measurements illustrate the breaking of radial trap symmetry in our trap due to gravity. This can be understood by considering that the atomic cloud sags under gravity to the point where the axial gradient of about 30 G/cm gives a force on atoms in the $|F = 1, m_F = -1\rangle$ equal to the gravitational force. By the condition $\vec{\nabla} \cdot \vec{B} = 0$, the presence of this axial gradient implies a radial field gradient of 15 G/cm which breaks the symmetry of the radial quadrupole field, adding to the magnetic field gradient along one direction ($\hat{y}$) while subtracting from that along the other direction ($\hat{x}$). Thus, triaxial, rather than cylindrically symmetric, traps are produced.

One motivating factor in our tailoring the aspect ratio of the IP trap is the desire to detect the presence of quantum depletion by precise measurements of collective excitation frequencies, as proposed by Stringari and Pitaevskii [29]. If one considers a fixed condensate number and axial trap strength, one finds that the largest magnitude frequency shift of the lowest collective mode would be obtained with traps that are nearly isotropic; even though higher condensate densities (and hence higher quantum depletion) are produced in prolate traps, the quadrupole modes in this case are more surface-like, rather than compressional, in character, and hence are only weakly affected by depletion effects. In our case, the broken symmetry due to effects of gravity produced, at best, nearly isotropic traps. For instance, Fig. 5 shows time-of-flight absorption images of atoms from a $\omega_x : \omega_y : \omega_z = 0.91 : 1.08 : 1.00$ trap. The familiar pronounced anisotropy of an expanding BEC is absent from such images due to the trap isotropy.

Another feature highlighted by the large axial confinement of our trap is a means to vary the orientation of the trap with respect to the nominal axial direction. This effect arises from considering the effects of displacing the radial quadrupole gradient field so that its zero-field axis no longer coincides with the axis of the curvature fields. That is, one considers the fields

$$\begin{aligned} \vec{B}_{curv} &= B_0 \hat{z} + \frac{B_z''}{2}\left[\left(z^2 - \frac{x^2+y^2}{2}\right)\hat{z} - z\,(x\hat{x} + y\hat{y})\right] \\ \vec{B}_{grad} &= B_\rho' \left[(x - x_0)\hat{x} - (y - y_0)\hat{y}\right] \end{aligned} \quad (1)$$

where (x_0, y_0) is the position of the gradient-preferred-axis in the $\hat{x}$ – $\hat{y}$ plane. This position is controlled experimentally by applying uniform radial fields to a well-aligned ($x_0 = y_0 = 0$) IP trap. Such misalignment yields both a variable displacement and variable tilt of the resulting magnetic trap, which can be understood as follows. Considering for now just the $z = 0$ plane, the location of the magnetic trap is determined by the competition between $\vec{B}_{grad}$, which tends to locate the cloud at (x_0, y_0), and the radial variation of the axial field $\vec{B}_{curv}$ which, for small displacements, exerts a radially repulsive force. The (x, y) position of the resulting field minimum

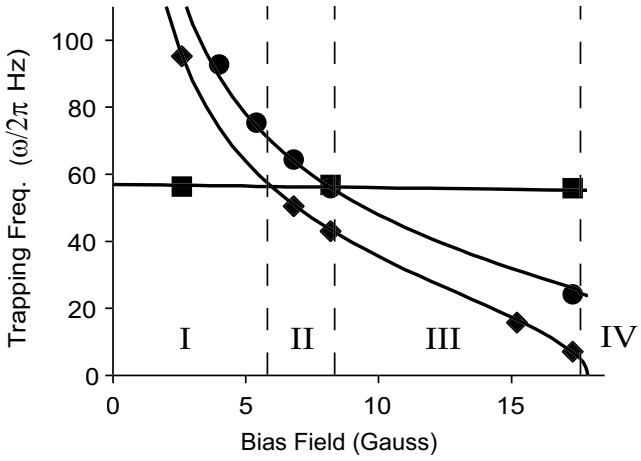

FIG. 4: Measured axial trapping frequency ω_z (squares) and transverse trapping frequencies ω_x (diamonds) and ω_y (circles) as a function of bias field, which was controlled by varying the current in the anti-bias coil pair. The solid lines are theoretical predictions for the trapping frequencies. The only free parameter in the transverse trapping frequency fit is the gradient coil contribution which was allowed to vary within its measured uncertainty. Four distinct regimes can be identified: I - the prolate spheroidal regime ("cigar"-shaped clouds), II - the nearly-isotropic regime, III - the oblate spheroidal regime ("pancake"-shaped), and IV - the unstable regime.

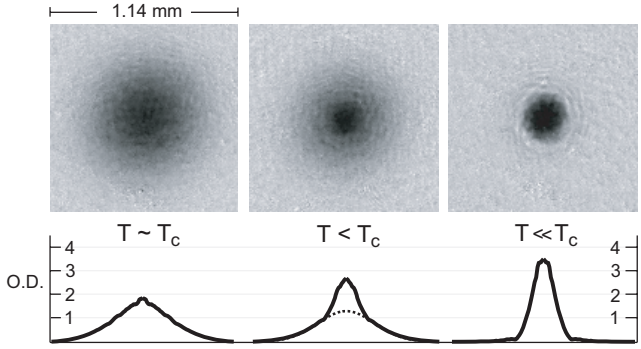

FIG. 5: Absorption images of a nearly-isotropic ultracold gas. Images show separate 36 ms time-of-flight images of a thermal cloud (1.5×10^6 atoms), bimodal distribution, and pure BEC (0.5×10^6 atoms), respectively. The trapping frequencies for this trap are $\{\omega_x, \omega_y, \omega_z\} = 2\pi \times \{52, 62, 57\}$Hz. Below the images are associated radial averages of the optical densities. The bimodal distribution (center plot) is clearly seen with the condensate rising from the Gaussian fit to the thermal wings (dotted line).

varies for $z \neq 0$ due to the fact that the $\vec{B}_{curv}$ fields now acquire radial components, displacing the position of the radial-field minimum from (x_0, y_0).

To illustrate this effect, we present in Fig. 6 the tilt angles θ with respect to the $\hat{z}$ axis of the weakest trap axis in a prolate IP trap, as derived from Eqs. 1. Field parameters of $B_z'' = 2000$ G/cm^2, $B_\rho' = 180$ G/cm, and displace-

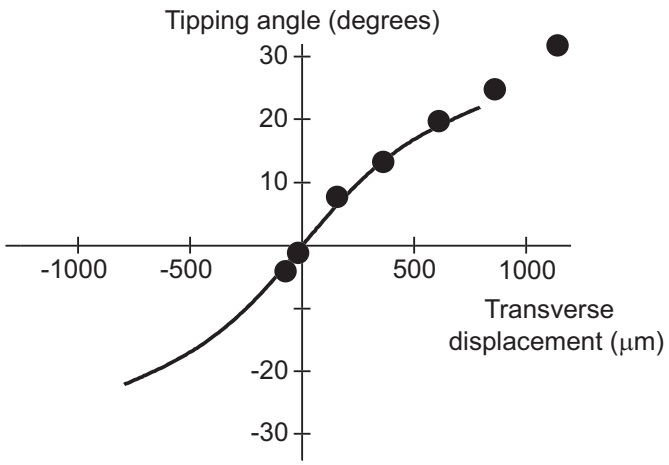

FIG. 6: Tilting atomic clouds in an IP magnetic trap. *In situ* images of tipped prolate clouds yield both the displacement (distinct from x_o) and the tipping angle (data shown as points). These data are compared with calculations (solid line) obtained from the generic IP field expressions of Eqs. 1 for the trap parameters of this experiment ($B_z'' = 2000$ G/cm^2, $B_\rho' = 180$ G/cm, and $y_0 = 0$). The theoretical curve is shown only over the range of displacements at which the IP traps (non-zero bias fields) are retained. Beyond this range, the displaced traps become filled, asymmetric spherical quadrupole traps, as presumably applies to the two data at highest displacements.

ments $y_0 = 0$ and variable x_0 are chosen to match experimental settings. The tilt angle varies over a wide range of x_0, out to a limiting displacement $x_c = 2\sqrt{B_0/B_z''}$ beyond which a non-zero-bias trap is no longer produced.

Aside from varying the tilt angle, this variation of the IP trap also changes the trap frequencies. Indeed, we observed experimentally that the "axial" trap frequency, i.e. the smallest frequency in a prolate IP trap, can be dramatically reduced in the case of a misalignment (x_0 and/or $y_0 \neq 0$). This leads to an apparent discrepancy between this trap frequency, which was determined by following the oscillatory motion of a trapped cloud, and a measurement of B_z'', as determined from measuring the upward ($\hat{z}$) displacement of the magnetic trap for a given axial field gradient, when the misalignment was large. Once external fields were applied to correct this misalignment, the measured trap frequencies and axial field curvatures were in agreement.

In conclusion, we have constructed a novel mm-scale IP magnetic trap which provides the means for tailoring magnetic potentials on length scales intermediate to the larger, inch-scale electromagnets and smaller microfabricated devices. The millimeter length scale is in some ways natural for manipulating cold atomic clouds, generating sufficiently deep and well behaved potentials over the ∼100 micron scale of typical gaseous samples. This trapping technology may thus provide a flexible means to transport ultracold clouds or construct large scale waveguides appropriate for condensate-based interferometry schemes [7, 30–32]. Further, making use of the strong axial confinement of the millitrap, we have demonstrated a wide range of trapping geometries which may enable a variety of experiments. For instance, the ability to continuously manipulate the tilt of a cigar-shaped condensate with respect to a fixed axis, simply by the application of uniform magnetic fields, provides a new all-magnetic method for imparting angular momentum to a trapped gas. Compared with laser-based excitation schemes, the utility of which is limited by the length scales of an optical focus (Rayleigh range, beam waist radius) [15], this method may allow the excitation of vortices in BECs with extremely small radial dimensions. Finally, the achievement of large BECs in the millitrap, which by design is compatible with existing technologies for high-finesse Fabry-Perot optical resonators, accomplishes a significant milestone toward the application of cavity quantum electrodynamics to magnetically trapped ultracold atoms.

We acknowledge the skillful work of Dave Murai and Armando Baeza of the UCB Physics Machine Shop in constructing and installing the mount pieces. The authors effort was sponsored by the Defense Advanced Research Projects Agency (DARPA) and Air Force Laboratory, Air Force Materiel Command, USAF, under Contract No. F30602-01-2-0524, the NSF (Grant No. 0130414), the Alfred P. Sloan and David and Lucile Packard Foundations, and the University of California. KLM acknowledges support from the National Science Foundation. SG acknowledges support from the Miller Institute for Basic Research in Science.

[1] M. H. Anderson *et al.*, Science **269**, 198 (1995).
[2] M.-O. Mewes *et al.*, Phys. Rev. Lett. **77**, 416 (1996).
[3] T. Esslinger, I. Bloch, and T. W. Hänsch, Phys. Rev. A **58**, R2664 (1998).
[4] D. M. Stamper-Kurn, H. J. Miesner, S. Inouye, M. R. Andrews, and W. Ketterle, Phys. Rev. Lett. **81**, 500 (1998).
[5] S. Dettmer *et al.*, Phys. Rev. Lett. **87**, 160406 (2001).
[6] H. J. Lewandowski, D. M. Harber, D. L. Whitaker, and E. A. Cornell, Phys. Rev. Lett. **88**, 070403 (2002).
[7] Y.-J. Wang *et al.*, preprint, ArXiV cond-mat/0407689.
[8] Y. Shin *et al.*, Phys. Rev. Lett. **93**, 160406 (2004).
[9] D. S. Durfee *et al.*, in *"Bose-Einstein condensation in atomic gases", Proceedings of the International School of Physics, Course CXL*, edited by M. Inguscio, S. Stringari, and C. E. Wieman (IOS Press, Amsterdam, 1999), pp. 67–176.
[10] R. Folman *et al.*, Phys. Rev. Lett. **84**, 4749 (2000).
[11] W. Hänsel, P. Hommelhoff, T. W. Hänsch, and J. Reichel,

Nature **413**, 498 (2001).
[12] H. Ott, J. Fortagh, G. Schlotterbeck, A. Grossmann, and C. Zimmermann, Phys. Rev. Lett. **87**, 230401 (2001).
[13] Specialized atom-chip traps have been fabricated which may give axial curvatures up to 10^8 G/cm^2 [33, 34] .
[14] O. M. Maragò *et al.*, Phys. Rev. Lett. **84**, 2056 (2000).
[15] K. W. Madison, F. Chevy, W. Wohlleben, and J. Dalibard, Phys. Rev. Lett. **84**, 806 (2000).
[16] J. R. Abo-Shaeer, C. Raman, J. M. Vogels, and W. Ketterle, Science **292**, 476 (2001).
[17] G. Hechenblaikner, E. Hodby, S. A. Hopkins, O. M. Marago, and C. J. Foot, Phys. Rev. Lett. **88**, 070406 (2002).
[18] S. Stringari, Phys. Rev. Lett. **86**, 4725 (2001).
[19] C. J. Hood, M. S. Chapman, T. W. Lynn, and H. J. Kimble, Phys. Rev. Lett. **80**, 4157 (1998).
[20] J. Ye, D. W. Vernooy, and H. J. Kimble, Phys. Rev. Lett. **83**, 4987 (1999).
[21] P. W. H. Pinske, T. Fischer, P. Maunz, and G. Rempe, Nature **404**, 365 (2000).
[22] M. Greiner, I. Bloch, T. W. Hänsch, and T. Esslinger, Phys. Rev. A **63**, 031401(R) (2001).
[23] J. Arlt *et al.*, J. Phys. B **32**, 5861 (1999).
[24] W. Ketterle and N. J. van Druten, in *Advances in Atomic, Molecular, and Optical Physics*, edited by B. Bederson and H. Walther (Academic Press, San Diego, 1996), Vol. 37, pp. 181 – 236.
[25] P. W. H. Pinkse *et al.*, Phys. Rev. A **57**, 4747 (1998).
[26] A. Gorlitz *et al.*, Phys. Rev. Lett. **87**, 130402 (2001).
[27] D. Rychtarik, B. Engeser, H.-C. Nägerl, and R. Grimm, Phys. Rev. Lett. **92**, 173003 (2004).
[28] N. L. Smith *et al.*, arXiv preprint cond-mat/0410101.
[29] L. Pitaevskii and S. Stringari, Phys. Rev. Lett. **81**, 4541 (1998).
[30] Y. Shin *et al.*, Phys. Rev. Lett. **92**, 050405 (2004).
[31] W. Hänsel, J. Reichel, P. Hommelhoff,and T. W. Hänsch, Phys. Rev. A **64**, 063607 (2001).
[32] E. Andersson *et al.*, Phys. Rev. Lett. **88**, 100401 (2002).
[33] B. Lev, Nanotechnology **15**, S556 (2004).
[34] M. Drndic *et al.*, Applied Physics Letters **72**, 2906 (1998).

Appendix G

Bose-Einstein Condensation in a Circular Waveguide

This appendix includes the following paper:

- *S. Gupta, K. W. Murch, K. L. Moore, T. P. Purdy, and D. M. Stamper-Kurn, Bose-Einstein condensation in a circular waveguide, Phys. Rev. Lett.* ***95****, 143201 (2005)*

Bose-Einstein Condensation in a Circular Waveguide

S. Gupta, K. W. Murch, K. L. Moore, T. P. Purdy, and D. M. Stamper-Kurn
Department of Physics, University of California, Berkeley, California 94720, USA
(Received 27 April 2005; published 29 September 2005)

We have produced Bose-Einstein condensates in a ring-shaped magnetic waveguide. The few-millimeter diameter, nonzero-bias ring is formed from a time-averaged quadrupole ring. Condensates that propagate around the ring make several revolutions within the time it takes for them to expand to fill the ring. The ring shape is ideally suited for studies of vorticity in a multiply connected geometry and is promising as a rotation sensor.

DOI: 10.1103/PhysRevLett.95.143201 PACS numbers: 39.20.+q, 03.75.−b, 05.30.Jp, 39.25.+k

The long range phase coherence of superfluids and superconductors, aside from leading to interesting physical effects, is also of practical importance in allowing for precise measurement devices based on quantum interference. In such devices, spatially separated paths forming a multiply connected geometry are imposed on the macroscopic quantum system. For example, a SQUID magnetometer makes use of a superconducting ring interrupted by Josephson junctions to allow continuous sensitivity to magnetic fields. A similar geometry was used in a superfluid ^{3}He gyroscope [1].

Dilute gas superfluids have now enabled novel forms of matter-wave interferometry. Precise sensors of rotation, acceleration, and other sources of quantal phases [2,3] using trapped or guided atoms have been envisioned. In particular, the sensitivity of atom-interferometric gyroscopes is proportional to the area enclosed by the closed loop around which atoms are guided [4]. Such considerations motivate the development of closed-loop atom waveguides that enclose a sizable area.

A number of multiply connected trapping geometries for cold atoms have been discussed. Optical traps using high-order Gauss-Laguerre beams were proposed [5,6], and hollow light beams were used to trap nondegenerate atoms in an array of small-radius rings [7]. Large-scale magnetic storage rings were developed for cold neutrons [8] and discussed for atomic hydrogen [9]. More recently, closed-loop magnetic waveguides were demonstrated for laser cooled atoms [10,11]. Unfortunately, these guides are characterized by large variations in the potential energy along the waveguide and by high transmission losses at points where the magnetic field vanishes.

In this Letter, we report the creation of a smooth, stable circular waveguide for ultracold atoms. A simple arrangement of coaxial electromagnetic coils was used to produce a static ring-shaped magnetic trap, which we call the quadrupole ring (Q ring), in which strong transverse confinement is provided by a two-dimensional quadrupole field. Atoms trapped in the Q ring experience large Majorana losses, but we can eliminate such losses with a time-orbiting ring trap (TORT) [12]. In this manner, stable circular waveguides with diameters ranging from 1.2 to 3 mm were produced. Finally, we report on the production of Bose-Einstein condensates (BECs) in a portion of the circular waveguide, and on the guiding of an ultracold atomic beam for several revolutions around the guide. This ring-shaped trap presents opportunities for studies of BECs that are homogeneous in one dimension and therefore of the unterminated propagation of sound waves [13] and solitons [14–16], of persistent currents [17–20], of quantum gases in low dimensions, and of matter-wave interferometry.

To explain the origin of the quadrupole ring trap, we consider a cylindrically symmetric static magnetic field $\vec{B}_c$ in a source-free region. Expanding $\vec{B}_c$ to low order about a point (taken as the origin) on the axis where the field magnitude has a local quadratic minimum, we have

$$\vec{B}_c = B_0\hat{z} + \frac{B_z''}{2}\left[\left(z^2 - \frac{x^2+y^2}{2}\right)\hat{z} - z(x\hat{x} + y\hat{y})\right], \quad (1)$$

where $B_0 > 0$ is the field magnitude at the origin, B_z'' is the

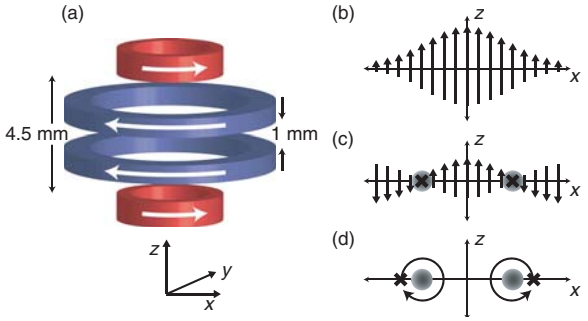

FIG. 1 (color). Forming a circular magnetic waveguide. (a) Four coaxial circular electromagnets (see [21] for details) are used to generate both the static (currents as shown) and rotating fields needed for the waveguide. Axes are indicated; gravity points along $-\hat{z}$. (b) As shown schematically, the field (arrows) from just the two outer coils (curvature coils, outer pair) points axially in the midplane between the coils, with largest fields at the axis. (c) Adding a uniform opposing bias field (using antibias coils, inner pair) produces a ring of field zeros (×) in the $\hat{x}$-$\hat{y}$ plane around which weak-field seeking atoms (shaded region) are trapped. (d) Rapidly rotating the field zeros around the trapped atoms produces the TORT.

axial field curvature, and Cartesian coordinates (x, y, z) are chosen so that z is the axial coordinate. The magnetic field magnitude falls to zero in the $\hat{x}$-$\hat{y}$ plane along a circle of radius $\rho_0 = 2\sqrt{B_0/B_z''}$ centered at the origin. This is the Q ring, a ring-shaped magnetic trap for weak-field seeking atoms. Near the field zeros, the magnetic field has the form of a transverse (radial and axial directions) two-dimensional quadrupole field with gradient $B' = \sqrt{B_0 B_z''}$. Such traps can also be obtained using different electromagnet configurations [12].

In our apparatus, the Q ring is formed using a subset of the coils (the curvature and antibias coils; see Fig. 1) used in our recently demonstrated millimeter-scale Ioffe-Pritchard magnetic trap [21]. Our work is aided, in particular, by the large axial curvatures produced in this trap and by the vertical orientation of the trap axis. These features are relevant for the operation of a Q ring in the presence of gravity, for two reasons. First, trapping atoms in the Q ring requires transverse confinement sufficient to overcome the force of gravity; this places a lower bound on the radius of the Q ring of $\rho_0 > \rho_{\min} \simeq 2mg/|\mu|B_z''$ with m the atomic mass, g the acceleration due to gravity, and μ the atomic magnetic moment. Indeed, if $\rho_{\min}$ exceeds the range over which Eq. (1) is valid, typically the distance to the field-producing coils, the formation of a Q ring may be precluded entirely. With $B_z'' = 5300$ G/cm^2 in our experiments, $\rho_{\min} = 115$ μm is much smaller than the millimeter dimensions of the electromagnets used for the trap. Second, the vertical orientation of the Q-ring axis allows cold atoms to move slowly along the nearly horizontal waveguide rather than being confined in a deep gravitational well.

Atoms can be localized to a particular portion of the Q ring by application of a uniform sideways (in the $\hat{x}$-$\hat{y}$ plane) magnetic field; e.g., a weak bias field $B_s\hat{x}$ tilts the Q ring by $\Delta z/\rho_0 = (B_s/B')/\rho_0$ about the $\hat{y}$ axis. This adjustment also adds an azimuthal field of magnitude $B_s|\sin\theta|$, splitting the Q ring into two trap minima at opposite sides of the ring, with θ being the azimuthal angle conventionally defined.

We loaded cold atoms into the Q ring using a procedure similar to previous work [21]. Briefly, about 2×10^9 ^{87}Rb atoms in the $|F = 1, m_F = -1\rangle$ hyperfine ground state were loaded into one of two adjacent spherical quadrupole magnetic traps. Using these traps, atoms were transported 3 inches from the loading region to the Q-ring trap region. During this transport, rf evaporative cooling was applied, yielding 2.5×10^7 atoms at a temperature of 60 μK in a spherical quadrupole trap with an axial field gradient of 200 G/cm. Within 1 s, we then converted the spherical quadrupole to a tilted Q-ring trap produced with $B_z'' = 5300$ G/cm^2, $B_0 = 22$ G, and a side field of magnitude $B_s = 9.2$ G. This process left 2×10^7 atoms trapped in the Q ring (Fig. 2).

The trapping lifetime of atoms in the Q ring is limited by Majorana losses. In a balanced Q ring, trapped atoms passing close to the line of zero field, which extends all around the ring, may flip their spins and be expelled from the trap. Extending the treatment by Petrich *et al.* [22] to this scenario, we estimate a Majorana loss rate of $\frac{\hbar^{1/2}}{\pi m^{3/4}} \times \frac{(\mu B')^{3/2}}{(k_B T)^{5/4}} = 6$ s^{-1} for our trap at a temperature of 60 μK. In a tilted Q ring, the zero-field region is reduced to just two points at opposite sides of the ring. Majorana losses in a tilted Q ring are thus similar to those in spherical quadrupole traps and much smaller than in a balanced Q ring. We confirmed this qualitative behavior by measuring the lifetime of trapped atoms in balanced and tilted Q-ring traps. In the balanced Q ring, the measured 0.3 s^{-1} Majorana loss rate was thrice that in a tilted Q ring, while falling far short of the predicted 6 s^{-1} loss rate, presumably due to residual azimuthal fields.

The high loss rates in the Q ring can be mended in a manner similar to the time-orbiting potential (TOP) trap by which Majorana losses in a spherical quadrupole field were overcome [22]. As proposed by Arnold [12], a TORT with nonzero bias field can be formed by displacing the ring of field zeros away from and then rapidly rotating it around the trapped atoms [Fig. 1(d)]. From Eq. (1), the Q ring can be displaced radially by application of an axial bias field, and displaced along $\hat{z}$ by a cylindrically symmetric spherical quadrupole field. The TORT provides transverse quadratic confinement with an effective field curvature of $B_{\text{eff}}'' = B'^2/2B_{\text{rot}}$, where B_{rot} is the magnitude of the rotating field seen at the trap minimum. Just as the TOP trap depth is limited by the "circle of death," the TORT trap

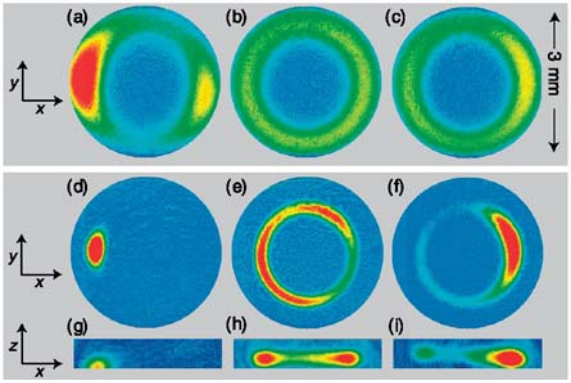

FIG. 2 (color). Atoms in a ring-shaped magnetic trap. Shown are top (a)–(f) and side (g)–(i) absorption images of ultracold ^{87}Rb clouds in either a Q ring (a)–(c) or TORT (d)–(i) with applied side field $B_s = 9.2$ (left), 0 (middle), and -2.5 G (right column), respectively, in the $\hat{x}$ direction. Images were taken 2 ms after turning off the traps. The applied field tilts the Q ring or TORT and favors atomic population in one side or another of the trap. For $B_s \sim 0$, the trap lies nearly in the horizontal plane and its azimuthal potential variation is minimized. For the Q ring, $B_0 = 22$ G; for the TORT, $B_0 = 20$ G and $B_{\text{rot}} = 17$ G; and $B_z'' = 5300$ G/cm^2 for both. The temperature of trapped atoms is 90 μK in the Q ring, and 10 μK in the TORT. Resonant absorption ranges from 0 (blue) to >80% (red).

depth is limited by a "torus of death," the locus of points at which the magnetic field is zero at some time [23]. This scheme may be applied equally to a tilted Q ring, yielding a tilted TORT and providing a stable trap in which atoms are confined to a portion of the ring. The sideways magnetic field (e.g., along $\hat{x}$) causes the magnetic potential minimum to vary azimuthally in the tilted TORT as $|\mu|\sqrt{B_{\rm rot}^2 + B_s^2 \sin^2\theta}$, while the gravitational potential is the same as that in a Q ring.

The time-varying fields needed to convert our Q ring (or tilted Q ring) traps to TORT (or tilted TORT) traps were obtained by suitably modulating the currents in the four coils used to generate the Q-ring potential. A modulation frequency of 5 kHz was chosen to be much larger than the transverse motional frequencies (< 100 Hz) and also much smaller than the Larmor frequency (> 3 MHz) at the location of the trap minimum. To first switch on the TORT, a rotating field magnitude of $B_{\rm rot} = 18$ G was used [24].

As shown in Fig. 3, the trap lifetime was dramatically increased by application of the TORT trap. In the first few seconds after switching on the TORT, we observed a fast loss of atoms and a simultaneous drop in their temperature. We ascribe this loss and cooling to the evaporation of atoms from the trapped cloud through the "torus of death." As the temperature dropped, the evaporation rate diminished and the lifetime of trapped atoms became vacuum limited at 90 s, a value observed both for balanced and for tilted TORT traps.

Given their longevity, it was possible to cool evaporatively the TORT-trapped atoms to the point of quantum degeneracy. Using a tilted TORT with $B_s \sim 9$ G, evaporation was performed in two stages. First, "torus of death" evaporation was applied by ramping down the rotating field strength $B_{\rm rot}$ over 40 s to 4.8 G. The oscillation frequencies in this trap were measured as $\omega_\perp = 2\pi \times (87, 74.5)$ Hz in the transverse and $\omega_\theta = 2\pi \times 35$ Hz in the azimuthal directions, in agreement with predictions [25]. In the second stage, rf evaporation was applied for 20 s, yielding clouds of up to 6×10^5 atoms at the Bose-Einstein condensation temperature, and pure BECs of up to 3×10^5 atoms.

Finally, to assess the suitability of the TORT as an atomic waveguide for interferometry, we launched our trapped BECs into closed-loop circular motion along the guide. This was accomplished by reorienting the sideways bias field B_s, inducing the trapped BEC to accelerate toward the newly positioned tilted TORT trap minimum (advanced by an azimuthal angle of about $\pi/4$), while simultaneously reducing the magnitude of B_s to $B_s \sim 0$ and increasing $B_{\rm rot}$ to 12.6 G to produce a well-balanced TORT trap. The TORT was then maintained at this setting, with radius $\rho_0 = 1.25$ mm ($B_0 = 20$ G, $B_z'' = 5300$ G/cm^2), and transverse trap frequencies of $\omega_\perp \simeq 2\pi \times 50$ Hz as measured at the launch point of the atoms. The atoms were allowed to propagate freely around the guide for various guiding times before being observed by absorption imaging. As shown in Fig. 4, the ultracold atomic beam propagated around the circular waveguide at an angular (linear) velocity of 40.5 rad/s (50.6 mm/s). As measured from the azimuthal extent of the atoms for different guiding times, this pulsed atom beam was characterized by an azimuthal rms velocity spread of 1.4 mm/s, equivalent to a longitudinal kinetic temperature

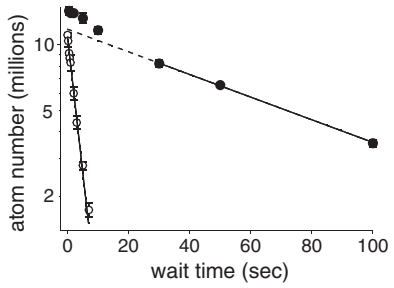

FIG. 3. Elimination of Majorana losses in the TORT. The measured number of trapped atoms in a Q ring (open circles) or TORT (solid circles) trap is shown vs residence time in the trap. Exponential fits indicate a 3 s Majorana-loss-limited lifetime in the Q ring. In the TORT, following an initial (30 s) loss of atoms due to evaporation, a vacuum limited lifetime of 90 s was observed. Settings for B_0, B_z'', and $B_{\rm rot}$ are as in Fig. 2, $B_s \sim 0$, and the initial temperature is 60 μK.

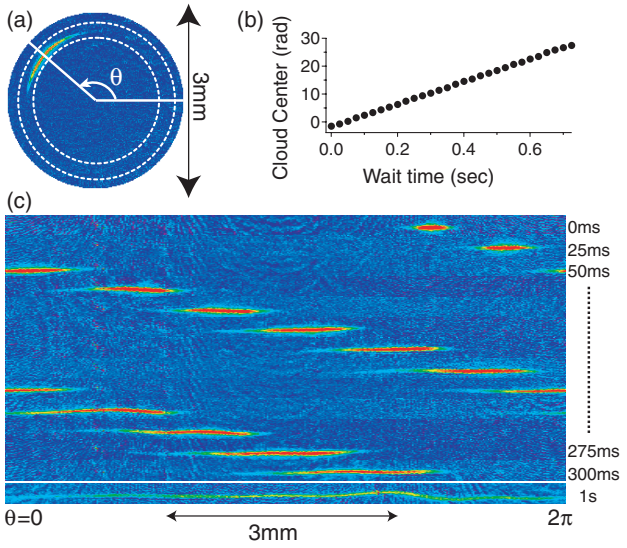

FIG. 4 (color). Circular motion of a quantum degenerate atomic beam in a waveguide. A Bose-Einstein condensate was launched into a balanced TORT and allowed to propagate. (a) Top view in-trap absorption image during the propagation. The mean azimuthal position of the BEC measured from such images is shown in (b). Annular portions (indicated by dashed circles) of top-view images taken at different guiding times are shown in (c) displayed in polar coordinates (radius vs azimuthal angle). The beam advances at an angular velocity of 40.5 rad/s while expanding due to an rms azimuthal velocity spread of 1.4 mm/s. After 1 s, the beam fills the entire guide.

of 22 nK. After about 1 s of guiding, this velocity variation caused the atomic cloud to spread throughout the waveguide, by which point the atoms had traveled $L = 51$ mm along the waveguide, encompassing an area of $A = L\rho_0/2 = 32$ mm^2. One would expect the front and back ends of the expanding BEC to interfere spatially as they overlap after 1 s of propagation in the guide. However, the fringe periodicity of ~600 nm expected for such interference is well below our imaging resolution of several μm, and we observed no such interference.

Many requisite elements for interferometric rotation sensing are still lacking in our system, including a means of in-guide coherent atomic beam splitting [26,27], bidirectional propagation, proper radial waveguiding [28], full characterization of longitudinal coherence in the beam, an assessment of the influence of the time-orbiting field on sensor precision, and atom-interferometric stability. Nevertheless, it is valuable to consider the possible sensitivity of our system if these elements are attained. As limited by atomic shot noise, rotation measurements with an uncertainty of $\Delta\Omega = (\hbar/4mA)N_0^{-1/2} \sim 1 \times 10^{-8}$ rad/s could be made from a single (1 s long) measurement, where $N_0 = 3 \times 10^5$ is the number of atoms used. While this figure is nearly 20 times that of existing atom-based gyroscopes [4], improvements such as launching the atoms at higher velocities, increasing the TORT radius, and increasing the atom number may ultimately yield a useful, compact sensing device.

Other applications of the TORT may include studies of propagation [29–31] and nonlinear dynamics [32] in atomic waveguides. In a TORT potential that is modified either by application of magnetic fields or by tilting with respect to gravity, BECs can be studied both undergoing pendular motion (terminated guide) when launched at small velocities, and undergoing circular motion (unterminated guide) at larger velocities.

Another appealing possibility is the study of BECs that fill the ring-shaped trap, rather than forming in just a portion of the ring. Such a system would allow for studies of quantized and persistent circulation [17–20], unterminated motion of solitons [14–16], and other aspects of nonlinear dynamics [33]. For this purpose, the azimuthal variation in the TORT potential must be reduced below the typical ~100 nK scale of the BEC chemical potential. From measurements of the kinetic energy of BEC's undergoing circular motion in our trap (data of Fig. 4), we estimate the TORT potential varied by as much as 5 μK. We believe this figure can be reduced greatly by using traps of smaller radius, by designing better electromagnets for both the static and the rotating fields used for the TORT, and also by controlling the orientation of the electromagnets with respect to gravity.

This work was sponsored by DARPA (Contract No. F30602-01-2-0524), the NSF (Grant No. 0130414), the David and Lucile Packard Foundation, and the University of California. K. L. M. acknowledges support from the NSF, and S. G. from the Miller Institute.

Note added.—After the submission of this paper, related work was reported by Arnold and collaborators [34].

[1] R. W. Simmonds *et al.*, Nature (London) **412**, 55 (2001).
[2] K. G. Petrosyan and L. You, Phys. Rev. A **59**, 639 (1999).
[3] Y. Lyanda-Geller and P. M. Goldbart, Phys. Rev. A **61**, 043609 (2000).
[4] T. Gustavson, A. Landragin, and M. Kasevich, Classical Quantum Gravity **17**, 2385 (2000).
[5] E. M. Wright, J. Arlt, and K. Dholakia, Phys. Rev. A **63**, 013608 (2001).
[6] B. P. Anderson, K. Dholakia, and E. M. Wright, Phys. Rev. A **67**, 033601 (2003).
[7] P. Verkerk and D. Hennequin, physics/0306155.
[8] K.-J. Kügler, K. Moritz, W. Paul, and U. Trinks, Nucl. Instrum. Methods Phys. Res. **228**, 240 (1985).
[9] D. Thompson, R. V. E. Lovelace, and D. M. Lee, J. Opt. Soc. Am. B **6**, 2227 (1989).
[10] J. A. Sauer, M. D. Barrett, and M. S. Chapman, Phys. Rev. Lett. **87**, 270401 (2001).
[11] S. Wu, W. Rooijakkers, P. Striehl, and M. Prentiss, Phys. Rev. A **70**, 013409 (2004).
[12] A. S. Arnold, J. Phys. B **37**, L29 (2004).
[13] M. R. Andrews *et al.*, Phys. Rev. Lett. **79**, 553 (1997).
[14] L. Salasnich, A. Parola, and L. Reatto, Phys. Rev. A **59**, 2990 (1999).
[15] J. Brand and W. P. Reinhardt, J. Phys. B **34**, L113 (2001).
[16] J.-P. Martikainen *et al.*, Phys. Rev. A **64**, 063602 (2001).
[17] F. Bloch, Phys. Rev. A **7**, 2187 (1973).
[18] J. Javanainen, S. M. Paik, and S. M. Yoo, Phys. Rev. A **58**, 580 (1998).
[19] M. Benakli *et al.*, Europhys. Lett. **46**, 275 (1999).
[20] E. Nugent, D. McPeake, and J. F. McCann, Phys. Rev. A **68**, 063606 (2003).
[21] K. L. Moore *et al.*, cond-mat/0504010.
[22] W. Petrich, M. H. Anderson, J. R. Ensher, and E. A. Cornell, Phys. Rev. Lett. **74**, 3352 (1995).
[23] Because of this topology, rf evaporation should be equally effective whether one approaches the Larmor frequency at the trap minimum from above or below.
[24] The magnitude of B_{rot} ranged between ~15 and 20 G during the 5 kHz modulation.
[25] The transverse asymmetry arises because of the sideways field.
[26] Y.-J. Wang *et al.*, Phys. Rev. Lett. **94**, 090405 (2005).
[27] S. Wu, E. J. Su, and M. Prentiss, cond-mat/0503130.
[28] E. Andersson *et al.*, Phys. Rev. Lett. **88**, 100401 (2002).
[29] K. Bongs *et al.*, Phys. Rev. A **63**, 031602(R) (2001).
[30] A. E. Leanhardt *et al.*, Phys. Rev. Lett. **89**, 040401 (2002).
[31] J. Fortàgh *et al.*, Appl. Phys. B **76**, 157 (2003).
[32] H. Ott *et al.*, Phys. Rev. Lett. **91**, 040402 (2003).
[33] L. J. Garay, J. R. Anglin, J. I. Cirac, and P. Zoller, Phys. Rev. Lett. **85**, 4643 (2000).
[34] A. S. Arnold, C. S. Garvie, and E. Riis, cond-mat/0506142.

Appendix H

Probing the Quantum State of a Guided Atom Laser Pulse

This appendix includes the following paper:

- *K. L. Moore, S. Gupta, K. W. Murch, and D. M. Stamper-Kurn, Probing the quantum state of a guided atom laser pulse, Phys. Rev. Lett. 97, 180401 (2006)*

Probing the Quantum State of a Guided Atom Laser Pulse

Kevin L. Moore,* Subhadeep Gupta, Kater W. Murch, and Dan M. Stamper-Kurn
Department of Physics, University of California, Berkeley, California 94720, USA
(Received 7 June 2006; published 2 November 2006)

We describe bichromatic superradiant pump-probe spectroscopy as a tomographic probe of the Wigner function of a dispersing particle beam. We employed this technique to characterize the quantum state of an ultracold atomic beam, derived from a ^{87}Rb Bose-Einstein condensate, as it propagated in a 2.5 mm diameter circular waveguide. Our measurements place an upper bound on the longitudinal phase space area occupied by the 3×10^5 atom beam of $9(1)\hbar$ and a lower bound on the coherence length of $\mathcal{L} \geq 13(1)$ μm. These results are consistent with full quantum degeneracy after multiple orbits around the waveguide.

DOI: 10.1103/PhysRevLett.97.180410 PACS numbers: 03.75.Pp, 32.80.−t, 42.50.Gy

Advances in the control of quantum degenerate gases have mirrored those of optical lasers, including the realization of high-contrast atom interferometers [1,2], nonlinear atom optics [3], and dispersion management [4,5]. Further, given single-mode waveguides [6] and other atom optical elements, the prospect of sensitive guided-atom interferometry has invited intensive experimental pursuit. Critical to realizing this prospect are methods for characterizing the coherence of a guided atom beam, akin to beam characterization in a high-energy particle accelerator.

Pulsed particle beams are naturally described by the Wigner quasiprobability distribution, defined as [7]

$$W(\mathbf{r}, \mathbf{p}) = \frac{1}{2\pi} \int e^{-i\mathbf{p}\cdot\mathbf{y}/\hbar} \left\langle \mathbf{r} - \frac{\mathbf{y}}{2} \middle| \hat{\rho} \middle| \mathbf{r} + \frac{\mathbf{y}}{2} \right\rangle d\mathbf{y}, \quad (1)$$

with $\hat{\rho}$ being the density matrix of the system. This distribution is the quantum mechanical equivalent of the classical phase space distribution. Experimentally, $W(\mathbf{r}, \mathbf{p})$ is determined tomographically by measuring its projection at various angles in phase space [8,9].

In this Letter we describe the use of bichromatic superradiant pump-probe spectroscopy (SPPS) to measure the Wigner function of an atomic beam propagating in a circular waveguide [10]. A form of such spectroscopy is applied to atoms in a circular waveguide, allowing for a measurement of the phase space density despite a significant coherent velocity chirp across the beam. Both long-range coherence and single transverse mode propagation were evident over many waveguide revolutions, implying that a guided atom laser pulse derived from a Bose-Einstein condensate remains coherent for at least 300 ms of propagation.

Superradiant light scattering from quantum degenerate gases provides striking confirmation of their long-range coherence [11,12]. An elongated cloud undergoing superradiance scatters light preferentially into "end-fire modes," leading to highly directional emission [13]. Coherence between scattered and unscattered atoms establishes a periodic grating of density or polarization which stimulates further light scattering. Once established, by superradiance or otherwise [14,15], this grating will decay or dephase on a time scale $\tau_c = m/2|\mathbf{q}|\sigma_p$ with m being the atomic mass, $\hbar\mathbf{q}$ the superradiant scattering recoil momentum, and σ_p the rms momentum spread of the unscattered atoms along the recoil direction. This can be isolated experimentally by applying superradiance in a pump-probe spectroscopic technique: after a first optical pump pulse initiates superradiance and establishes coherence in the gas, this coherence is allowed to decay freely for a time τ before a second optical pulse is applied. In Ref. [12], this technique revealed in detail the bimodal momentum distribution of a partly condensed Bose gas.

Let us consider applying such spectroscopy to a beam of N atoms in the transverse ground state of a 1D waveguide with longitudinal rms spatial and momentum widths of σ_x and σ_p, respectively. The 1D Wigner function of the beam is bounded by these widths to occupy a phase space area of $\mathcal{A}_{\max} = \sigma_x\sigma_p$. However, $\mathcal{A}_{\max}$ may represent a gross overestimate of the actual phase space area occupied by the beam. For example, assume that the beam originates from a thermally equilibrated trapped gas that was released into the waveguide. Free expansion causes the momentum and position of the beam to be strongly correlated, a feature captured by a posited Wigner function of the form

$$W(x, p) = \frac{\exp\left[-\frac{1}{2(1-\eta^2)}\left(\frac{x^2}{\sigma_x^2} - 2\eta\frac{xp}{\sigma_x\sigma_p} + \frac{p^2}{\sigma_p^2}\right)\right]}{\pi\sigma_x\sigma_p\sqrt{1-\eta^2}}, \quad (2)$$

where $\eta = \langle px\rangle/\sigma_p\sigma_x$ (Fig. 1). The actual phase space area $\mathcal{A}$ of such a beam is smaller than the aforementioned estimate by a factor $\sqrt{1-\eta^2}$. That is, for proper characterization of a beam one must distinguish between a spatially inhomogeneous momentum width σ_p, which may be dominated by a coherent velocity chirp across the length of the beam, and a "homogeneous" width $\mathcal{A}/\sigma_x$.

To access these correlations, we consider *bichromatic* SPPS in which the recoil momenta $\hbar\mathbf{q}_1$ and $\hbar\mathbf{q}_2$ imparted

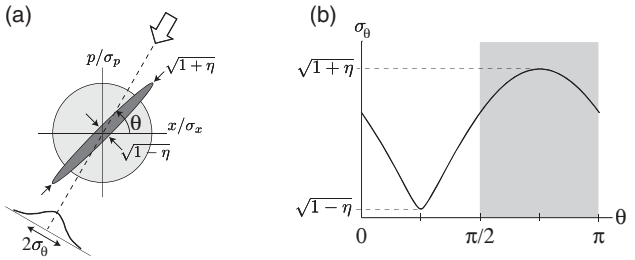

FIG. 1. Projective measurements as probes of quantum degeneracy. (a) Contours of Gaussian Wigner distributions $W(x, p)$ are shown. $W(x, p)$ is determined by its projections at all angles $0 \leq \theta < \pi$. Measurements of only the momentum and position distributions ($\theta = 0$ and $\theta = \pi/2$ projections, respectively), cannot distinguish a homogeneous (light shading) from a correlated ensemble (dark shading). (b) rms widths of distributions derived at various projection angles are shown. Time-of-flight analyses recover a limited range of projection angles (shaded), while bichromatic SPPS accesses all projection angles.

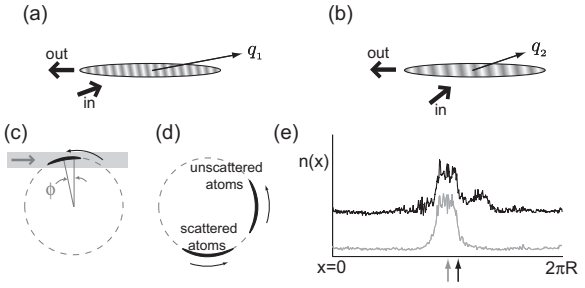

FIG. 2. Bichromatic SPPS in a circular waveguide. (a) Superradiant Rayleigh scattering of a pump pulse establishes a density modulation of wave vector $\hbar\mathbf{q}_1$ in an elongated atomic beam. (b) A coherent velocity chirp causes the modulation wave vector to decrease along the long axis. The remaining coherence is revealed by light scattering with recoil momentum $\hbar\mathbf{q}_2$ matched to the modified density grating. (c) Pump (probe) light illuminates the freely propagating atom beam at angle ϕ ($\phi + \Omega\tau$) relative to the mean angular position, and (d) scattered atoms separate from the original pulse and can be distinguished from unscattered atoms. (e) Azimuthal density distributions $n(x)$ in the ring 160 ms after illumination are shown for beams that have (black) or have not (gray) undergone superradiant light scattering. The shifted center of mass (indicated by arrows) quantifies the total superradiant scattering rate.

by superradiance are different for the pump and probe pulses, respectively (Fig. 2). These differing momenta may result experimentally from pump and probe pulses which differ in wave vector, or, as in the present experiment, which differ in their angle of incidence with respect to the long axis of the cloud. Restricting our treatment to one dimension along $\hat{x}$, the superradiant scattering rate Γ from the second (probe) light pulse [11,16] can be expressed in terms of the Wigner function of the state of the system *before* the first (pump) pulse as

$$\Gamma \propto \left| \iint e^{i(\frac{q_1\tau}{m}p + \Delta q x)} W(x, p) dx dp \right|^2, \qquad (3)$$

where $\Delta q = q_2 - q_1$ with $\hbar q_1$ and $\hbar q_2$ being the projections of the recoil momenta along the $\hat{x}$ axis, and τ is the pump-probe delay time. Performing an extended canonical transformation to generalized coordinates $\tilde{x} = (x/\sigma_x) \times \cos\theta + (p/\sigma_p)\sin\theta$ and $\tilde{p} = -(x/\sigma_x)\sin\theta + (p/\sigma_p) \times \cos\theta$, with $\tan\theta = -\frac{\Delta q m}{q_1 \tau}\frac{\sigma_x}{\sigma_p}$ we obtain

$$\Gamma \propto \left| \int e^{i(\frac{\sigma_p q_1 \tau}{m}\cos\theta - \sigma_x \Delta q \sin\theta)\tilde{p}} d\tilde{p} \int W(x, p) d\tilde{x} \right|^2. \qquad (4)$$

Monochromatic SPPS ($\Delta q = 0$) yields information only on the overall momentum distribution of the atomic system, which derives from projecting the Wigner function on the momentum axis ($\theta = 0$) [12]. In contrast, bichromatic SPPS assesses the Wigner function at a nonzero projection angle θ. In particular, tuning experimental parameters such that $\theta = \pi/4$ probes the Wigner function of Eq. (2) along the narrow axis corresponding to the linear momentum chirp across the cloud, and thereby provides a sensitive measurement of η and of the phase space density of the beam. In this case the observed coherence time is increased to $\tau_c = m/2|\mathbf{q}|\sigma_p\sqrt{1-\eta}$.

In other words, in monochromatic SPPS the reduction of the superradiant scattering rate from a linearly chirped beam comes about mainly by dephasing. The density modulation established by the pump pulse evolves at a frequency which is Doppler-shifted upward on one end and downward on the other end of the momentum-chirped beam. This causes the wave vector of the density modulation to decrease linearly with time. In bichromatic SPPS, by matching the recoil momentum of the probe pulse to the wave vector of the density grating, we recover a superradiant scattering rate which reveals the remaining homogeneous decay of motional coherence.

We now turn to our implementation of this scheme to probe a pulsed atom laser beam in a circular waveguide. This beam originated from a ^{87}Rb Bose-Einstein condensate of 3×10^5 atoms produced in a magnetic time-orbiting ring trap (TORT) [10,17], biased to yield a three-dimensional harmonic trap with trapping frequencies $(\omega_x, \omega_T) = 2\pi \times (35, 85)$ s^{-1} in the longitudinal (i.e., azimuthal in the ring) and transverse directions, respectively. These atoms were launched azimuthally by adiabatically decompressing the trap to $\omega_x = 2\pi \times 6$ s^{-1} and displacing the trap minimum to a new longitudinal position for 30 ms, accelerating the cloud to a mean orbital angular frequency $\Omega = 2\pi \times 8.4$ s^{-1} chosen to be far from any betatron resonances [17]. The TORT potential was then balanced over the next 30 ms and operated with radius $R = 1.25$ mm and ω_T as above. The launched atomic beam was allowed to propagate freely in this circular guide.

While the beam's provenance as a Bose-Einstein condensate suggests its full coherence at later times, it may also be argued that heating from trap vibrations and imperfections, collisions with background gas particles, or effects related to the quasi-1D nature of the guided atoms

[18] can indeed cause the coherence to be spoiled after sufficient propagation times. Thus, our experimental goal was to measure quantitatively the coherence of this propagating atom beam at an arbitrary time after its launch.

We made use of direct absorption imaging of the propagating atom beam to discern several properties of its evolution. Such imaging, applied along the symmetry axis of the circular waveguide, quantified the longitudinal linear density of the beam $n(x)$ [Fig. 2(c)]. From the growth of the spatial width σ_x of the beam vs propagation time, we determined the rms momentum width as $\sigma_p = m \times 1.8$ mm/s, a value within 10% of that expected due to the release of interaction energy in the launched Bose-Einstein condensate. The transverse state of the atomic beam was characterized by suddenly releasing the atom beam from the waveguide and imaging the transverse extent of the beam after variable times of flight. These observations agreed well with a mean-field model of the coherent expansion of a Bose-Einstein condensate into a tight waveguide [19], and indicated the transverse state of the beam to be the ground state of the harmonic transverse confining potential after about 150 ms of propagation. The beam can thus be treated as one-dimensional with its azimuthal state remaining unknown. Combining these observations, we obtain an upper bound on the longitudinal phase space area of $\mathcal{A}_{\max} = 310\hbar$ for the beam after a half-revolution in the guide given its $\sigma_x = 120$ μm rms width at that stage.

This constraint on $\mathcal{A}_{\max}$ was dramatically improved by application of SPPS to the propagating beam. The probe and pump pulses were both obtained from a single laser source propagating in the plane of the waveguide (to within $\pm 1°$) with a 0.4 mm beam diameter, a detuning 560 MHz below the $^2S_{1/2}, F = 1 \rightarrow {}^2P_{3/2}, F = 0$ transition, and circular polarization. Typical intensities were 10 mW/cm^2, corresponding to observed single-particle Rayleigh scattering rates of 400 s^{-1}, and pulses were typically 50 μs in duration. After application of the light pulses, the atoms were allowed to propagate in the waveguide until the scattered atoms had clearly separated from the unscattered atoms. The fraction of scattered atoms and, hence, the total superradiant scattering rate from the pump-probe sequence, was then determined from the center-of-mass of the beam ($x_{\text{c.m.}}$) in the azimuthal coordinate.

Such pump-probe spectroscopy was applied to the atom beam at different propagation times, and thus at different locations in the circular guide. As shown in Fig. 3, the measured coherence times depend strongly on the position of the beam in the guide. Letting ϕ measure the central angular position of the beam away from the point at which the pump/probe light is tangential to the guide, the superradiant response of atoms at large angles ($|\phi| \gtrsim 20°$) decays after a pump-probe delay time of around 50 μs, consistent with the coherence time discussed above for monochromatic SPPS determined by the overall momentum width of the beam. In contrast, for beam positions

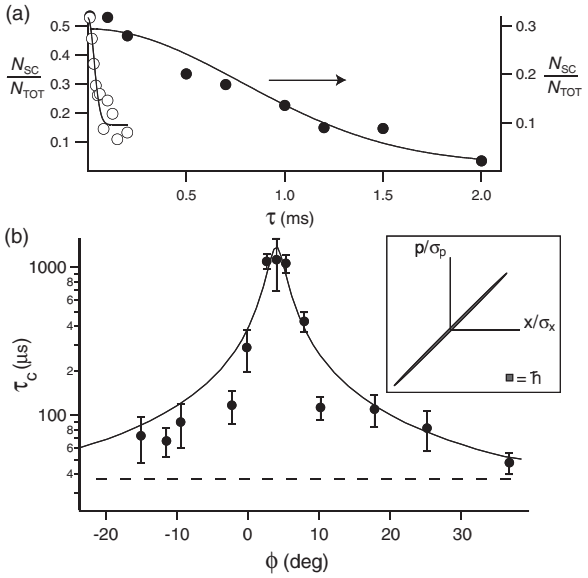

FIG. 3. Bichromatic SPPS of a quantum degenerate beam at approximately a half-revolution in the circular waveguide. (a) SPPS at $\phi = 38°$ (open circles) and $\phi = 4°$ (closed circles) gives coherence times $\tau_c = 47(8)$ μs and 1.1(1) ms, respectively, defined by the $1/e$ decay time of the superradiant signal (Gaussian fits to data are shown). (b) Measured coherence times are compared to theoretical predictions for a coherent Gaussian beam (solid line) and an incoherent, uncorrelated ensemble (dotted line). The theoretical curve in fact predicts the maximum coherence time at $\phi = 31°$ (see text), but has been shifted for comparison to data. The inset shows the Wigner distribution implied by the 1.1 ms coherence time. A phase space cell of area $\hbar$ is included for reference.

closer to $\phi = 4°$, the coherence time is dramatically increased to over 1 ms, indicating coherence in the beam beyond that implied solely by the overall momentum width. Similar coherence times were observed after one, two, and three full revolutions around the ring.

This strong geometric dependence can be understood in the context of bichromatic SPPS. During the time τ between application of the pump and probe pulses, the propagating atom beam rotates by an angle $\Omega\tau$, thereby varying the relative orientation between the incident light and the end-fire superradiant emission from the gas. Expressed in a frame corotating with the atom beam, the superradiant recoil momenta of the pump and probe beams differ by $\Delta\mathbf{q} \simeq k\Omega\tau(-\sin\phi\hat{x} + \cos\phi\hat{r})$, with $\hat{x}$ and $\hat{r}$ being unit vectors in the azimuthal and radial transverse directions, respectively, and assuming $\Omega\tau \ll 1$. Thus, the pump-probe wave vector difference Δq, which is needed for tomographic measurements of the Wigner function, is not established by varying the incident probe light; rather, Δq arises from the rotation of the atomic beam, and thereby of the wave vector of "end-fire mode" light emission, during the delay time.

We now apply the one-dimensional treatment of bichromatic SPPS to this situation by considering just the con-

tribution of longitudinal phase matching to superradiant scattering. SPPS applied to the rotating beam while at an angle ϕ probes the Wigner function of the beam at a *constant* phase space projection angle given by $\tan\theta = \frac{m\Omega\sigma_x}{\sigma_p}\frac{\sin\phi}{1+\cos\phi}$. Different projections of θ are thus obtained merely by measuring τ_c at different positions ϕ of the beam. We note that while these measurements of τ_c do not constitute a complete tomography of the Wigner function, they do allow us to reconstruct an ellipsoid which bounds the phase space occupied by the beam. Under this approximation that $W(x, p)$ is indeed Gaussian, our measurements do suffice for complete tomographic reconstruction. With better data quality, our technique could be used to reconstruct a Wigner function of a more general form.

Using experimentally measured quantities for the beam after a half-revolution in the waveguide, the condition $\tan\theta = 1$ for probing the homogeneous momentum width of the correlated atom beam is predicted to occur at $\phi_c = 31°$. This value clearly does not match the experimentally observed $\phi_c = 4(2)°$ [Fig. 3(b)]. 2D models which numerically evaluated the superradiance phase-matching integral [11] showed that the beam curvature alone did not resolve this disagreement. Rather, to account for this discrepancy, we suspect it is necessary to adapt our 1D treatment of superradiance to beams with small Fresnel number, i.e., with length greatly exceeding the Rayleigh range defined by the probe wavelength and the transverse width of the atom beam. We suspect that our method may be probing only short portions of the beam, the momentum width of which is enhanced by their small extent, rather than probing the beam as a whole.

Despite the imperfect match between the 1D theory and the experimental data, the most important prediction of bichromatic SPPS in a rotating system—long coherence times at $\phi > 0$—is clearly evident in this system. We thus assert that the observations retain their relevance as a probe of the phase space distribution of the atom beam. From the maximum coherence time of $\tau_c = 1.1(1)$ ms, we obtain an empirical value of $\eta = 1 - [4.9(6) \times 10^{-4}]$ for the aforementioned correlation parameter. The atom beam is thus constrained to inhabit a phase space area of $\mathcal{A} = 9(1)\hbar$, equivalent to placing a lower bound of $\mathcal{L} = (\hbar|\mathbf{q}|/m)\tau_c = 13(1)\ \mu$m [14] on the longitudinal coherence length of the propagating cloud.

The maximum coherence time observed is plausibly limited not by the lack of longitudinal coherence, but rather by the decay of the superradiant scattering rate $\Gamma(\tau)$ due to transverse phase matching. Assessing a 2D phase-matching integral with the transverse state being the noninteracting ground state of the transverse trapping potential, one finds an upper bound on the coherence time of $\approx(2\Omega k\sigma_T\cos\phi)^{-1} < 1200\ \mu$s, with $\sigma_T = \sqrt{\hbar/2m\omega_T}$ and ω_T being the transverse trap frequency. Thus, our observations should be construed as placing quantitative lower bounds on the coherence of the propagating atom beam while remaining consistent with its complete coherence.

This work was supported by DARPA (Contract No. F30602-01-2-0524), ARO, and the David and Lucile Packard Foundation. K. L. M. acknowledges support from NSF and S. G. from the Miller Institute.

*Electronic address: klmoore@berkeley.edu

[1] S. Gupta, K. Dieckmann, Z. Hadzibabic, and D. E. Pritchard, Phys. Rev. Lett. **89**, 140401 (2002).
[2] Y. Torii, Y. Suzuki, M. Kozuma, T. Sugiura, T. Kuga, L. Deng, and E. W. Hagley, Phys. Rev. A **61**, 041602(R) (2000).
[3] L. Deng, E. W. Hagley, J. Wen, M. Trippenbach, Y. Band, P. S. Julienne, J. E. Simsarian, K. Helmerson, S. L. Rolston, and W. D. Phillips, Nature (London) **398**, 218 (1999).
[4] B. Eiermann, P. Treutlein, Th. Anker, M. Albiez, M. Taglieber, K.-P. Marzlin, and M. K. Oberthaler, Phys. Rev. Lett. **91**, 060402 (2003).
[5] B. Eiermann, Th. Anker, M. Albiez, M. Taglieber, P. Treutlein, K.-P. Marzlin, and M. K. Oberthaler, Phys. Rev. Lett. **92**, 230401 (2004).
[6] A. E. Leanhardt, A. P. Chikkatur, D. Kielpinski, Y. Shin, T. L. Gustavson, W. Ketterle, and D. E. Pritchard, Phys. Rev. Lett. **89**, 040401 (2002).
[7] E. Wigner, Phys. Rev. **40**, 749 (1932).
[8] D. Leibfried, D. M. Meekhof, B. E. King, C. Monroe, W. M. Itano, and D. J. Wineland, Phys. Rev. Lett. **77**, 4281 (1996).
[9] C. Kurtsiefer, T. Pfau, and J. Mlynek, Nature (London) **386**, 150 (1997).
[10] S. Gupta, K. W. Murch, K. L. Moore, T. P. Purdy, and D. M. Stamper-Kurn, Phys. Rev. Lett. **95**, 143201 (2005).
[11] S. Inouye, A. P. Chikkatur, D. M. Stamper-Kurn, J. Stenger, and W. Ketterle, Science **285**, 571 (1999).
[12] Y. Yoshikawa, Y. Torii, and T. Kuga, Phys. Rev. Lett. **94**, 083602 (2005).
[13] N. E. Rehler and J. E. Eberly, Phys. Rev. A **3**, 1735 (1971).
[14] B. Saubaméa, T. W. Hijmans, S. Kulin, E. Rasel, E. Peik, M. Leduc, and C. Cohen-Tannoudji, Phys. Rev. Lett. **79**, 3146 (1997).
[15] S. Inouye, R. F. Löw, S. Gupta, T. Pfau, A. Görlitz, T. L. Gustavson, D. E. Pritchard, and W. Ketterle, Phys. Rev. Lett. **85**, 4225 (2000).
[16] J.-Y. Courtois, S. Guibal, D. R. Meacher, P. Verkerk, and G. Grynberg, Phys. Rev. Lett. **77**, 40 (1996).
[17] K. W. Murch, K. L. Moore, S. Gupta, and D. M. Stamper-Kurn, Phys. Rev. Lett. **96**, 013202 (2006).
[18] K. Bongs, S. Burger, S. Dettmer, D. Hellweg, J. Arlt, W. Ertmer, and K. Sengstock, Phys. Rev. A **63**, 031602(R) (2001).
[19] L. Salasnich, A. Parola, and L. Reatto, Phys. Rev. A **65**, 043614 (2002).

Bibliography

[1] D. M. Stamper-Kurn and W. Ketterle. Spinor condensates and light scattering from Bose-Einstein condensates. In R. Kaiser, C. Westbrook, and F. David, editors, *Coherent Matter Waves*, pages 137 – 218. Springer-Verlag, New York, 2001.

[2] W. Zhang, D. L. Zhou, M.-S. Chang, M. S. Chapman, and L. You. Dynamical Instability and Domain Formation in a Spin-1 Bose-Einstein Condensate. *Phys. Rev. Lett.*, 95(18):180403, 2005.

[3] Q. Gu, K. Bongs, and K. Sengstock. Spin waves in ferromagnetically coupled spinor Bose gases. *Phys. Rev. A*, 70(6), 2004.

[4] L. E. Sadler, J. M. Higbie, S. R. Leslie, M. Vengalattore, and D. M. Stamper-Kurn. Spontaneous symmetry breaking in a quenched ferromagnetic spinor Bose condensate. *Nature*, 443:312, 2006.

[5] A. T. Black, E. Gomez, L. D. Turner, S. Jung, and P. D. Lett. Spinor Dynamics in an Antiferromagnetic Spin-1 Condensate, 13 April 2007. arXiv:cond-mat/0704.0925.

[6] S. Richard, F. Gerbier, J. H. Thywissen, M. Hugbart, P. Bouyer, and A. Aspect. Momentum Spectroscopy of 1D Phase Fluctuations in Bose-Einstein Condensates. *Phys. Rev. Lett.*, 91:010405, 2003.

[7] T. Kinoshita, T. R. Wenger, and D. S. Weiss. Observation of a one-dimensional Tonks-Girardeau gas. *Science*, 305:1125, 2004.

[8] B. L. Tolra, K. M. O'Hara, J. H. Huckans, W. D. Phillips, S. L. Rolston, and J. V.

Porto. Observation of Reduced Three-Body Recombination in a Correlated 1D Degenerate Bose Gas. *Phys. Rev. Lett.*, 92(19):190401–4, 2004.

[9] Z. Hadzibabic, P. Krüger, M. Cheneau, B. Battelier, and J. Dalibard. Berezinskii-Kosterlitz-Thouless crossover in a trapped atomic gas. *Nature*, 441:1118, 2006.

[10] A. Griesmaier, J. Werner, S. Hensler, J Stuhler, and T. Pfau. Bose-Einstein Condensation of Chromium. *Phys. Rev. Lett.*, 94:160401, 2005.

[11] S. Giovanazzi, P. Pedri, L. Santos, A. Griesmaier, M. Fattori, T. Koch, J. Stuhler, and T. Pfau. Expansion dynamics of a dipolar Bose-Einstein Condensate. *Phys. Rev. A*, 74:013621, 2006.

[12] M. Greiner, O. Mandel, T. Esslinger, T. W. Hänsch, and I. Bloch. Quantum phase transition from a superfluid to a Mott insulator in a gas of ultracold atoms. *Nature*, 415:39, 2002.

[13] M. Greiner, I. Bloch, O. Mandel, T. W. Hänsch, and T. Esslinger. Exploring Phase Coherence in a 2D Lattice of Bose-Einstein Condensates. *Phys. Rev. Lett.*, 87:160405, 2001.

[14] S. Gupta, K. Dieckmann, Z. Hadzibabic, and D. E. Pritchard. Contrast interferometry using Bose-Einstein condensates to measure h/m and alpha. *Phys. Rev. Lett.*, 89:140401, 2002.

[15] B. DeMarco and D. S. Jin. Onset of Fermi degeneracy in a trapped atomic gas. *Science*, 285:1703, 1999.

[16] C. A. Regal, M. Greiner, and D. S. Jin. Observation of Resonance Condensation of Fermionic Atom Pairs. *Phys. Rev. Lett.*, 92:040403, 2004.

[17] M. W. Zwierlein, C. A. Stan, C. H. Schunck, S. M. F. Raupach, A. J. Kerman, and W. Ketterle. Condensation of Pairs of Fermionic Atoms near a Feshbach Resonance. *Phys. Rev. Lett.*, 92:120403, 2004.

[18] M. W. Zwierlein, J. R. Abo-Shaeer, A. Schirotzek, C. H. Schunck, and W. Ketterle. Vortices and superfluidity in a strongly interacting Fermi gas. *Nature*, 435(7045):1047–1051, 2005.

[19] M. Vengalattore, J. M. Higbie, S. R. Leslie, J. Guzman, L. E. Sadler, and D. M. Stamper-Kurn. High-resolution magnetometry with a spinor Bose-Einstein condensate. *Phys. Rev. Lett.*, 98:200801, 2007.

[20] C. J. Pethick and H. Smith. *Bose-Einstein Condensation in Dilute Gases*. Cambridge University Press, Cambridge, United Kingdom, 2002.

[21] D. M. Stamper-Kurn. *Peeking and poking at a new quantum fluid: studies of gaseous Bose-Einstein condensates in magnetic and optical traps*. Ph.d. thesis, Massachusetts Institute of Technology, 2000.

[22] E. P. Gross. *Nuovo Cimento*, 20:454, 1961.

[23] L. P. Pitaevskii. *Soviet Physics JETP*, 13:451, 1961.

[24] B. Eiermann, P. Treutlein, T. Anker, M. Albiez, M. Taglieber, K.-P. Marzlin, and M. K. Oberthaler. Dispersion Management for Atomic Matter Waves. *Phys. Rev. Lett.*, 91(6):060402, 2003.

[25] M. Albiez, R. Gati, J. Folling, S. Hunsmann, M. Cristiani, and M. K. Oberthaler. Direct Observation of Tunneling and Nonlinear Self-Trapping in a Single Bosonic Josephson Junction. *Phys. Rev. Lett.*, 95(1):010402, 2005.

[26] D. J. Heinzen. Ultracold atomic interactions. In M. Inguscio, S. Stringari, and C.E. Wieman, editors, *Bose-Einstein condensation in atomic gases*, Proceedings of the International School of Physics "Enrico Fermi," Course CXL, pages 351 – 390. IOS Press, Amsterdam, 1999.

[27] S. Inouye, M. R. Andrews, J. Stenger, H.-J. Miesner, D. M. Stamper-Kurn, and W. Ketterle. Observation of Feshbach Resonances in a Bose-Einstein Condensate. *Nature*, 392:151–154, 1998.

[28] D.-I. Choi and Q. Niu. Bose-Einstein condensates in an optical lattice. *Phys. Rev. Lett.*, 82(10):2022–5, 1999.

[29] T. P. Meyrath, F. Schreck, J. L. Hanssen, C.-S. Chuu, and M. G. Raizen. *Phys. Rev. A*, 71:041604(R), 2005.

[30] B. P. Anderson and M. A. Kasevich. Macroscopic Quantum Interference from Atomic Tunnel Arrays. *Science*, 282:1686, 1998.

[31] C. Orzel, A. K. Tuchman, M. L. Fenselau, M. Yasuda, and M. A. Kasevich. Squeezed States in a Bose-Einstein Condensate. *Science*, 291:2386, 2001.

[32] L. Mandel and E. Wolf. *Optical Coherence and Quantum Optics*. Cambridge University Press, Cambridge, United Kingdom, 1997.

[33] G. Nogues, A. Rauschenbeutel, S. Osnaghi, N. Brune, J. M. Raimond, and S. Haroche. Seeing a single photon without destroying it. *Nature*, 400:239, 1999.

[34] J. Vuckovic and Y Yamamoto. Photonic-crystals microcavities for cavity quantum electrodynamics with a single quantum dot. *Appl. Phys. Lett.*, 82:2374, 2003.

[35] A. Blais, H. R.-S. Huang, A. Wallraff, S. M. Girvin, and R. J. Schoelkopf. Cavity quantum electrodynamics for superconducting electrical circuits: an architecture for quantum computation. *Phys. Rev. A*, 69:62320, 2004.

[36] A. Wallraff, D. I. Schuster, A. Blais, L. Frunzio, R.-S. Huang, J. Majer, S. Kumar, S. M. Girvin, and R. J. Schoelkopf. Strong coupling of a single photon to a superconducting qubit using circuit quantum electrodynamics. *Nature*, 431:162, 2004.

[37] J. M. Raimond, M. Brune, and S. Haroche. Colloquium: Manipulating quantum entanglement with atoms and photons in a cavity. *Rev. Mod. Phys.*, 73(3):565, 2001.

[38] C. J. Hood, M. S. Chapman, T. W. Lynn, and H. J. Kimble. Real-time cavity QED with single atoms. *Phys. Rev. Lett.*, 80(19):4157, 1998.

[39] J. Ye, D. W. Vernooy, and H. J. Kimble. Trapping of single atoms in cavity QED. *Phys. Rev. Lett.*, 83:4987, 1999.

[40] C. J. Hood, T. W. Lynn, A. C. Doherty, A. S. Parkins, and H. J. Kimble. The atom-cavity microscope: single atoms bound in orbit by single photons. *Science*, 287:1447, 2000.

[41] J. McKeever, J. R. Buck, A. D. Boozer, A. Kuzmich, H.-C. Nagerl, D. M. Stamper-Kurn, and H. J. Kimble. State-insensitive cooling and trapping of single atoms in an optical cavity. *Phys. Rev. Lett.*, 90:133602, 2003.

[42] J. McKeever, A. Boca, A. D. Boozer, J. R. Buck, and H. J. Kimble. Experimental realization of a one-atom laser in the regime of strong coupling. *Nature*, 425:268, 2003.

[43] A. Boca, R. Miller, K. M. Birnbaum, A. D. Boozer, J. McKeever, and H. J. Kimble. Observation of the Vacuum Rabi Spectrum for One Trapped Atom. *Phys. Rev. Lett.*, 93:233603, 2004.

[44] P. W. H. Pinkse, T. Fischer, P. Maunz, and G. Rempe. Trapping an atom with single photons. *Nature*, 404:365, 2000.

[45] M. Hennrich, T. Legero, A. Kuhn, and G. Rempe. Vacuum-stimulated Raman scattering based on adiabatic passage in a high-finesse optical cavity. *Phys. Rev. Lett.*, 85:4872, 2000.

[46] A. B. Mundt, A. Kreuter, C. Becher, D. Liebried, J. Eschner, F. Schmidt-Kaler, and R. Blatt. Coupling a single atomic quantum bit to a high finesse optical cavity. *Phys. Rev. Lett.*, 89:103001, 2002.

[47] G. R. Guthohrlein, M. Keller, K. Hayasaka, W. Lange, and H. Walther. A single ion as a nanoscopic probe of an optical field. *Nature*, 414:49, 2002.

[48] A. B. Mundt, A. Kreuter, C. Russo, C. B. C, D. Leibfried, J. Eschner, F. S.-K. F, and R. Blatt. Coherent coupling of a single Ca-40^+ ion to a high-finesse optical cavity. *Applied Physics B - Lasers*, 76(2):117, 2003.

[49] J. A. Sauer, K. M. Fortier, M. S. Chang, C. D. Hamley, and M. S. Chapman. Cavity QED with optically transported atoms. *Phys. Rev. A*, 69:51804, 2004.

[50] A. Ottl, S. Ritter, M. Kohl, and T. Esslinger. Correlations and Counting Statistics of an Atom Laser. *Phys. Rev. Lett.*, 95(9):090404–4, 2005.

[51] A. Kuhn, M. Hennrich, and G. Rempe. Deterministic single-photon source for distributed quantum networking. *Phys. Rev. Lett.*, 89:067901, 2002.

[52] S. Gupta, K. W. Murch, K. L. Moore, T. P. Purdy, and D. M. Stamper-Kurn. Bose-Einstein Condensation in a Circular Waveguide. *Phys. Rev. Lett.*, 95(14):143201, 2005.

[53] K. W. Murch, K. L. Moore, S. Gupta, and D. M. Stamper-Kurn. Dispersion Management Using Betatron Resonances in an Ultracold-Atom Storage Ring. *Phys. Rev. Lett.*, 96(1):013202, 2006.

[54] K. L. Moore, T. P. Purdy, K. W. Murch, K. R. Brown, K. Dani, S. Gupta, and D. M. Stamper-Kurn. Bose-Einstein condensation in a mm-scale Ioffe-Pritchard trap. *Applied Physics B: Lasers and Optics*, pages DOI: 10.1007/s00340–005–2101–1, 2006.

[55] K. L. Moore, S. Gupta, K. W. Murch, and D. M. Stamper-Kurn. Probing the quantum state of a guided atom laser pulse. *Phys. Rev. Lett.*, 97:180401, 2006.

[56] A. K. Tuchman, R. Long, G. Vrijsen, J. Boudet, J. Lee, and M. A. Kasevich. Normal-mode splitting with large collective cooperativity. *Phys. Rev. A*, 74:053821, 2006.

[57] H. J. Metcalf and P. van der Straten. *Laser Cooling and Trapping*. Springer-Verlag, New York, 1999.

[58] A. Chikkatur. *Colliding and Moving Bose-Einstein Condensates: Studies of superfluidity and optical tweezers for condensate transport*. Ph.d. thesis, Massachusetts Institute of Technology, 2002.

[59] D. E. Pritchard. Trapping and Cooling Neutral Atoms. In D.C. Lorents, W.E. Meyerhof, and J.R. Peterson, editors, *Electronic and atomic collisions : invited papers*

of the XIV International Conference on the Physics of Electronic and Atomic Collisions, Palo Alto, California, 24-30 July, 1985, pages 593–604. Elsevier, New York, 1986.

[60] N. R. Newbury, C. J. Myatt, and C. E. Wieman. s-wave elastic collisions between cold ground-state 87Rb atoms. *Phys. Rev. A*, 51:R2680, 1995.

[61] K. B. MacAdam, A. Steinbach, and C. Wieman. A narrow-band tunable diode laser system with grating feedback, and a saturated absorption spectrometer for Cs and Rb. *Am. J. Phys.*, 60:12, 1992.

[62] W. Demtröder. *Laser Spectroscopy - Basic Concepts and Instrumentation*. Springer, New York, 2002.

[63] J. M. Higbie. *First Steps toward Precision Measurements using Multicomponent Bose-Einstein Condensates of Rb-87*. Ph.d. thesis, University of California, Berkeley, 2005.

[64] H. J. Lewandowski. *Coherences and correlations in an ultracold Bose gas*. Ph.d. thesis, University of Colorado, Boulder, 2002.

[65] K. L. Moore, T. P. Purdy, K. W. Murch, S. Leslie, S. Gupta, and D. M. Stamper-Kurn. Collimated, single-pass atom source from a pulsed alkali metal dispenser for laser-cooling experiments. *Review of Scientific Instruments*, 76:023106, 2005.

[66] L. E. Sadler. *Dynamics of a Spin 1 Ferromagnetic Condensate*. Ph.d. thesis, University of California, Berkeley, 2006.

[67] W. D. Phillips, J. V. Prodan, and H. J. Metcalf. Zeeman slowing. *J. Opt. Sci. Am. B*, 2:1751, 1985.

[68] T. E. Barrett, S. W. Dapore-Schwartz, M. D. Ray, and G. P. Lafyatis. Inverted Zeeman slower. *Phys. Rev. Lett.*, 67:3483, 1991.

[69] W. Ketterle, D. S. Durfee, and D. M. Stamper-Kurn. Making, probing and understanding Bose-Einstein condensates. In M. Inguscio, S. Stringari, and C.E. Wieman,

editors, *Bose-Einstein condensation in atomic gases*, Proceedings of the International School of Physics "Enrico Fermi," Course CXL, pages 67–176. IOS Press, Amsterdam, 1999.

[70] S. Chu, L. Hollberg, J. E. Bjorkholm, A. Cable, and A. Ashkin. Three-Dimensional Viscous Confinement and Cooling of Atoms by Resonance Radiation Pressure. *Phys. Rev. Lett.*, 55:48, 1985.

[71] M. Greiner, I. Bloch, T. W. Hänsch, and T. Esslinger. Magnetic transport of trapped cold atoms over a large distance. *Phys. Rev. A*, 63:031401, 2001.

[72] H. Mabuchi and A. C. Doherty. Cavity quantum electrodynamics: coherence in context. *Science*, 298:1372, 2002.

[73] Research Electro-Optics, Inc., 5505 Airport Blvd., Boulder, CO, 80301.

[74] Kimble H.J. Ye J. Hood, C. J. Characterization of high-finesse mirrors: Loss, phase shifts, and mode structure in an optical cavity. *Phys. Rev. A*, 64:033804, 2001.

[75] R. Folman, P. Krüger, D. Cassettari, B. Hessmo, T. Maier, and J. Schmiedmayer. Controlling Cold Atoms using Nanofabricated Surfaces: Atom Chips. *Phys. Rev. Lett.*, 84:4749, 2000.

[76] W. Hänsel, P. Hommelhoff, T. W. Hänsch, and J. Reichel. Bose-Einstein condensation on a microelectronic chip. *Nature*, 413:498, 2001.

[77] H. Ott, J. Fortagh, G. Schlotterbeck, A. Grossmann, and C. Zimmermann. Bose-Einstein Condensation in a Surface Microtrap. *Phys. Rev. Lett.*, 87:230401, 2001.

[78] D. R. Lide and ed. *CRC Handbook of Chemistry and Physics, 87th edition*. CRC Press, 2007.

[79] J. T. Watt and J. D. Plummer. Effect of interconnection delay on liquid nitrogen temperature CMOS circuit performance. *IEEE - Proceedings of the International Electronic Devices Meeting*, 87:393–396, 1987.

[80] J. Arlt, O. Marago, E. Hodby, S. A. Hopkins, G. Hechenblaikner, S. Webster, and C. J. Foot. Bose-Einstein condensation in a rotating anisotropic TOP trap. *Journal of Physics B-Atomic Molecular and Optical Physics*, 32(24):5861–5869, 1999.

[81] W. Ketterle and N. J. van Druten. Evaporative cooling of trapped atoms. In B. Bederson and H. Walther, editors, *Advances in Atomic, Molecular, and Optical Physics*, volume 37, pages 181 – 236. Academic Press, San Diego, 1996.

[82] P. W. H. Pinkse, A. Mosk, W. Weidmuller, M. W. Reynolds, and T. W. Hijmans. One-dimensional evaporative cooling of magnetically trapped atomic hydrogen. *Phys. Rev. A*, 57(6):4747, 1998.

[83] M. H. Anderson, J. R. Ensher, M. R. Matthews, C. E. Wieman, and E. A. Cornell. Observation of Bose-Einstein Condensation in a Dilute Atomic Vapor. *Science*, 269:198, 1995.

[84] W. Petrich, M. H. Anderson, J. R. Ensher, and E. A. Cornell. A Stable, Tightly Confining Magnetic Trap for Evaporative Cooling of Neutral Atoms. *Phys. Rev. Lett.*, 74:3352, 1995.

[85] A. S. Arnold. Adaptable-radius, time-orbiting magnetic ring trap for BoseEinstein condensates. *J. Phys. B*, 37:L29, 2004.

[86] D. W. Kerst and R. Serber. Electronic Orbits in an Induction Accelerator. *Phys. Rev.*, 60:53, 1961.

[87] T. Gustavson, A. Landragin, and M. Kasevich. Rotation sensing with a dual atom-interferometer Sagnac gyroscope. *Classical and Quantum Gravity*, 17:2385, 2000.

[88] M. G. Sagnac. *C. R. Acad. Sci.*, 157:708, 1913.

[89] J. A. Sauer, M. D. Barrett, and M. S. Chapman. Storage ring for neutral atoms. *Phys. Rev. Lett.*, 87:270401, 2001.

[90] S. Wu, W. Rooijakkers, P. Striehl, and M. Prentiss. Bidirectional propagation of cold atoms in a "stadium"-shaped magnetic guide. *Phys. Rev. A*, 70:013409, 2004.

[91] A. S. Arnold, C. S. Garvie, and E. Riis. preprint, arXiv:cond-mat/0506142.

[92] A. E. Leanhardt, A. P. Chikkatur, D. Kielpinski, Y. Shin, T. L. Gustavson, W. Ketterle, and D. E. Pritchard. Propagation of Bose-Einstein Condensates in a Magnetic Waveguide. *Phys. Rev. Lett.*, 89:040401, 2002.

[93] P. J. Martin, B. G. Oldaker, A. H. Miklich, and D. E. Pritchard. Bragg scattering of atoms from a standing light wave. *Phys. Rev. Lett.*, 60(6):515, 1988.

[94] P. L. Gould, G. A. Ruff, and D. E. Pritchard. Diffraction of atoms by light: the near–resonant Kapitza–Dirac effect. *Phys. Rev. Lett.*, 56(8):827, 1986.

[95] M. Kozuma, L. Deng, E. W. Hagley, J. Wen, R. Lutwak, K. Helmerson, S. L. Rolston, and W. D. Phillips. Coherent splitting of Bose–Einstein condensed atoms with optically induced Bragg diffraction. *Phys. Rev. Lett.*, 82(5):871, 1999.

[96] J. Stenger, S. Inouye, A. P. Chikkatur, D. M. Stamper-Kurn, D. E. Pritchard, and W. Ketterle. Bragg Spectroscopy of a Bose-Einstein condensate. *Phys. Rev. Lett.*, 82:4569, 1999.

[97] M. Saba, T. A. Pasquini, C. Sanner, Y. Shin, W. Ketterle, and D. E. Pritchard. Optical measurement of the phase of a Bose-Einstein condensate. *Science*, 307:1945, 2005.

[98] Y.-J. Wang, D. Z. Anderson, V. M. Bright, E. A. Cornell, Q. Diot, T. Kishimoto, M. Prentiss, R. A. Saravanan, S. R. Segal, and S. Wu. An Atom Michelson Interferometer on a Chip Using a Bose-Einstein Condensate. *Phys. Rev. Lett.*, 94:090405, 2005.

[99] O. Garcia, B. Deissler, K. J. Hughes, J. M. Reeves, and C. A. Sackett. Preprint arXiv:cond-mat/0603772 v2.

[100] P. L. Kapitza and P. A. M. Dirac. The reflection of electrons from standing light waves. *Prof. of the Camb. Philos. Soc.*, 29:297, 1933.

[101] S. Gupta. *Experiments with Degenerate Bose and Fermi Gases*. Ph.d. thesis, Massachusetts Institute of Technology, 2003.

[102] M. Abramowitz and eds. Stegun, A. *Handbook of Mathematical Functions with Formulas, Graphs, and Mathematical Tables*. Dover, New York, 1965.

[103] S. Wu, Y.-J. Wang, Q. Diot, and M. Prentiss. Splitting matter waves using an optimized standing-wave light-pulse sequence. *Phys. Rev. A*, 71:043602, 2005.

[104] K. Bongs, S. Burger, S. Dettmer, D. Hellweg, J. Arlt, W. Ertmer, and K. Sengstock. Waveguide for Bose-Einstein condensates. *Phys. Rev. A*, 63:031602(R), 2001.

[105] L. Salasnich, A. Parola, and L. Reatto. Effective wave equations for the dynamics of cigar-shaped and disk-shaped Bose condensates. *Phys. Rev. A*, 65(4):043614, 2002.

[106] K. Huang. *Statistical Mechanics*. Wiley, New York, second edition edition, 1987.

[107] J. Binney and S. Tremaine. *Galactic Dynamics (Princeton Series in Astrophysics)*. Princeton University Press, New Jersey, 1988.

[108] S. Turner, editor. *CAS - CERN Acclerator School: 5th General Accelerator Physics Course*. CERN, Geneva, Switzerland, 1994.

[109] S. Gupta, Z. Hadzibabic, J. R. Anglim, and W. Ketterle. Collisions in zero temperature Fermi gases. *Phys. Rev. Lett.*, 92:100401, 2004.

[110] E. Wigner. On the Quantum Correction For Thermodynamic Equilibrium. *Phys. Rev.*, 40(5):749, 1932.

[111] M. Hillery, R. F. O'Connell, M. O. Scully, and E. P. Wigner. Distribution Functions in Physics: Fundamentals. *Physics Reports (Review Section of Physics Letters)*, 106:121–167, 1984.

[112] H. Wallis, A. Röhrl, M. Naraschewski, and A. Schenzle. Phase space dynamics of Bose condensates: Interference vs. Interaction. *Phys. Rev. A*, 55:2109, 1997.

[113] N. Wheeler. Phase Space and Quantum Mechanics. Reed College, unpublished lecture notes.

[114] Y. S. Kim and M. E. Noz. *Phase Space Picture of Quantum Mechanics: Group Theoretical Approach*. World Scientific Publishing Company, New Jersey, 1991.

[115] R. N. Bracewell. Numerical Transforms. *Science*, 248:697–704, 1990.

[116] R. H. Dicke. Coherence in spontaneous radiation processes. *Phys. Rev.*, 93(1):99, 1954.

[117] S. Inouye, A. P. Chikkatur, D. M. Stamper-Kurn, J. Stenger, and W. Ketterle. Superradiant Rayleigh scattering from a Bose–Einstein condensate. *Science*, 285(July 23):571, 1999.

[118] S. Inouye, R. F. Löw, S. Gupta, T. Pfau, A. Görlitz, T. L. Gustavson, D. E. Pritchard, and W. Ketterle. Amplification of light and atoms in a Bose-Einstein condensate. *Phys. Rev. Lett.*, 85:4225, 2000.

[119] M. G. Moore and P. Meystre. Theory of Superradiant Scattering of Laser Light from Bose-Einstein Condensates. *Phys. Rev. Lett.*, 83:5202, 1999.

[120] W. Ketterle and S. Inouye. Does Matter Wave Amplification Work for Fermions? *Phys. Rev. Lett.*, 86(19):4203–4206, 2001.

[121] Y. Yoshikawa, Y. Torii, and T. Kuga. Superradiant Light Scattering from Thermal Atomic Vapors. *Phys. Rev. Lett.*, 94:083602, 2005.

[122] N. E. Rehler and J. H. Eberly. Superradiance. *Phys. Rev. A*, 3(5):1735, 1971.

[123] B. Saubamea, T. W. Hijmans, S. Kulin, E. Rasel, E. Peik, M. Leduc, and C. Cohen-Tannoudji. Direct measurement of the spatial correlation function of ultracold atoms. *Phys. Rev. Lett.*, 79(17):3146, 1997.

[124] R. Loudon. *The Quantum Theory of Light*. Clarendon, Oxford, 2nd edition edition, 1983.

[125] E. Jaynes and F. W. Cummings. *Proc. IEEE*, 51:89, 1963.

[126] R. J. Brecha, P. R. Rice, and M. Xiao. N two-level atoms in a driven optical cavity: Quantum dynamics of forward photon scattering for weak incident fields. *Phys. Rev. A*, 59:2392, 1999.

[127] M. Tavis and F. W. Cummings. Exact solution for an N-molecule-radiation-field Hamiltonian. *Phys. Rev.*, 170:379, 1968.

[128] D. W. Vernooy and H. J. Kimble. Well-dressed states for wave-packet dynamics in cavity QED. *Phys. Rev. A*, 56:4287, 1997.

[129] S. Leslie, N. Shenvi, K. R. Brown, D. M. Stamper-Kurn, and K. B. Whaley. Transmission Spectrum of an Optical Cavity Containing N Atoms. *Phys. Rev. A*, 69:043805, 2004.

[130] M. D. Lukin, S. F. Yelin, and M. Fleischhauer. Entanglement of Atomic Ensembles by Trapping Correlated Photon States. *Phys. Rev. Lett.*, Volume 84(Number 18):4232–4235, 2000.

[131] M. D. Lukin. Colloquium: Trapping and manipulating photon states in atomic ensembles. *Rev. Mod. Phys.*, 75:457, 2003.

[132] A. Kuzmich, W. P. Bowen, A. D. Boozer, A. Boca, C. W. Chou, L.-M. Duan, and H. J. Kimble. Generation of nonclassical photon pairs for scalable quantum communication with atomic ensembles. *Nature*, 423:731, 2003.

[133] H. W. Chan, A. T. Black, and V. Vuletić. Observation of Collective-Emission-Induced Cooling of Atoms in an Optical Cavity. *Phys. Rev. Lett.*, 90:063003, 2003.

[134] C. W. Chou, S. V. Polyakov, A. Kuzmich, and H. J. Kimble. Single-Photon Generation from Stored Excitation in an Atomic Ensemble. *Phys. Rev. Lett.*, 92:213601, 2004.

[135] D. A. Steck, 14 October 2003. Rubidium-87 D Line Data (unpublished, http://steck.us/alkalidata/).

[136] Puppe T. Schuster I. Syassen N. Pinkse P.W. H. Rempe G. Maunz, P. Normal-Mode Spectroscopy of a Single-Bound-Atom–Cavity System. *Phys. Rev. Lett.*, 94:033002–1 – 033002–4, 2005.

[137] J. McKeever, J. Buck, A. Boozer, and H. Kimble. Determination of the Number of Atoms Trapped in an Optical Cavity. *Phys. Rev. Lett.*, 93:143601, 2004.

[138] P. Berman, editor. *Cavity quantum electrodynamics*. Academic Press, Boston, 1994.

[139] E. Hecht. *Optics*. Addison-Wesley, Reading, 2nd edition edition, 1989.

[140] L. M. Duan, M. D. Lukin, J. I. Cirac, and P. Zoller. Long-distance quantum communication with atomic ensembles and linear optics. *Nature*, 414:413, 2001.

[141] A. S. Sorensen and K. Molmer. Entangling atoms in bad cavities. *Phys. Rev. A*, 66:022314, 2002.

[142] Y. Shimizu, N. Shiokawa, N. Yamamoto, M. Kozuma, T. Kuga, L. Deng, and E. W. Hagley. Control of Light Pulse Propagation with Only a Few Cold Atoms in a High-Finesse Microcavity. *Phys. Rev. Lett.*, 89:233001, 2002.

[143] A. I. Oliva, V. Sosa, R. de Coss, R. Sosa, N. Lopez-Salazar, and J. L. Pena. *Rev. Sci. Instruments*, 63:3326, 1992.

[144] K. W. Murch, K. L. Moore, S. Gupta, and D. M. Stamper-Kurn. in preparation.

[145] R. Grimm, M. Weidemüller, and Y. Ovchinnikov. Optical Dipole Traps for Neutral Atoms. Technical report, 1999.

[146] J. D. Miller, R. A. Cline, and D. J. Heinzen. Far-off-resonance optical trapping of atoms. *Phys. Rev. A*, 47:R4567, 1993.

[147] D. M. Stamper-Kurn, M. R. Andrews, A. P. Chikkatur, S. Inouye, H.-J. Miesner, J. Stenger, and W. Ketterle. Optical Confinement of a Bose-Einstein Condensate. *Phys. Rev. Lett.*, 80:2072–2075, 1998.

[148] S. Gupta, K. W. Murch, K. L. Moore, and D. M. Stamper-Kurn. in preparation.

[149] C.-S. Chuu, F. Schreck, T. P. Meyrath, J. L. Hanssen, G. N. Price, and M. G. Raizen. Direct Observation of Sub-Poissonian Number Statistics in a Degenerate Bose Gas. *Phys. Rev. Lett.*, 95:260403, 2005.

[150] J. Geremia, J. K. Stockton, and H. Mabuchi. Real-Time Quantum Feedback Control of Atomic Spin-Squeezing. *Science*, 204:270, 2004.